Published in final edited form as:
Sci Signal. ; 6(272): ra26. doi:10.1126/scisignal.2003312.

Pheromone-Induced Morphogenesis Improves Osmoadaptation Capacity by Activating the HOG MAPK Pathway**

Rodrigo Baltanás[1], **Alan Bush**[1], **Alicia Couto**[2], **Lucía Durrieu**[1], **Stefan Hohmann**[3], and **Alejandro Colman-Lerner**[1,*]

[1]Instituto de Fisiología, Biología Molecular y Neurociencias, Consejo Nacional de Investigaciones Científicas y Técnicas y Departamento de Fisiología, Biología Molecular y Celular, Facultad de Ciencias Exactas y Naturales, Universidad de Buenos Aires, Buenos Aires, Argentina

[2]CIHIDECAR-Departamento de Química Orgánica, Facultad de Ciencias Exactas y Naturales, Universidad de Buenos Aires, Buenos Aires, Argentina

[3]Department of Cell and Molecular Biology, University of Gothenburg, Gothenburg, Sweden

Abstract

Environmental and internal conditions expose cells to a multiplicity of stimuli whose consequences are difficult to predict. Here, we investigate the response to mating pheromone of yeast cells adapted to high osmolarity. Events downstream of pheromone binding involve two mitogen-activated protein kinase (MAPK) cascades: the pheromone response (PR) and the cell-wall integrity response (CWI). Although these MAPK pathways share components with each and a third MAPK pathway, the high osmolarity response (HOG), they are normally only activated by distinct stimuli, a phenomenon called insulation. We found that in cells adapted to high osmolarity, PR activated the HOG pathway in a pheromone- and osmolarity- dependent manner. Activation of HOG by the PR was not due to loss of insulation, but rather a response to a reduction in internal osmolarity, which resulted from an increase in glycerol release caused by the PR. By analyzing single-cell time courses, we found that stimulation of HOG occurred in discrete bursts that coincided with the “shmooing” morphogenetic process. Activation required the polarisome, the cell wall integrity MAPK Slt2, and the aquaglyceroporin Fps1. HOG activation resulted in high glycerol turnover that improved adaptability to rapid changes in osmolarity. Our work shows how a differentiation signal can recruit a second, unrelated sensory pathway to enable responses to yeast to multiple stimuli.

INTRODUCTION

Signal transduction systems have been traditionally studied in single input conditions. However, natural environments often present multiple stimuli that simultaneously activate several regulatory systems. The responses elicited by these systems might be contradictory, for instance when cells are simultaneously exposed to growth promoting and growth

*To whom correspondence should be addressed: colman-lerner@fbmc.fcen.uba.ar.

AUTHOR CONTRIBUTIONS: RB performed most of the experiments, and constructed most of the strains used in the study. AC measured glycerol content of samples. Together with RB, AB performed Hog1-venus nuclear localization, and volume recovery experiments. AB performed all the statistical analysis of the data. LD made strain LD3342. RB processed all the data of the paper. RB, AB and ACL analyzed the results. RB and ACL and wrote the paper. SH contributed to framing the research questions, interpretation of the data and edited the manuscript.

arresting stimuli. Little is known about how cells integrate such information to make adaptive decisions.

In haploid *S. cerevisiae*, two of the four mitogen-activated protein kinase (MAPK)-based systems (Fig. 1A), the high osmolarity glycerol (HOG) (1) and the cell wall integrity (CWI) (2), maintain homeostasis against environmental and developmental changes. The other two MAPK systems, the mating pheromone response (PR) (3) and the filamentation system (4), control developmental transitions in response to mating pheromone and certain nutritional metabolites, respectively.

Pheromones secreted by haploid yeast cells of opposite mating type (a factor and α, secreted by *MAT*a and *MAT*α cells) trigger a cell fate decision that leads to mating, which involves a G-protein coupled receptor and a scaffolded MAPK cascade that activates the extracellular signal-regulated kinase (ERK) 1/2-like MAPKs Fus3 and Kss1 (3) (Fig. 1A, left). The pathway is activated in *MAT*a cells when α factor binds to the receptor Ste2, ultimately culminating in the activation of the MAPKs Fus3 and Kss1. Activated Fus3 and Kss1 regulate cytoplasmic and nuclear targets, resulting in the induction of approximately 100 genes (5). Fus3 and Kss1 stimulate actin polarization towards the pheromone source, leading to a cell-shaping process called “shmooing”. This type of polarized cellular growth requires the assembly of a multi-protein complex called polarisome at the site of polarization. Deletion of some of its components, such as Spa2 and Pea2, does not affect the performance of the MAPK cascade or polarization itself (6) but prevents the formation of the characteristic narrow, pointy shmoos exhibited by wild-type cells. Shmooing stresses the cell wall, leading to activation of the CWI MAPK cascade (7–9) (Figure 1A). The CWI response mediates the turnover of cell wall material (2) and is activated by many stimuli, including hypo-osmotic shock, cell-wall disruptors, heat shock and pheromone treatment. Mucin-like proteins connecting the plasma membrane and cell wall serve as sensors and indirectly activate protein kinase C (PKC) in yeast, resulting in stimulation of the Bck1, Mkk1 and Mkk2, Slt2 MAPK cascade and modulation of transcription by Slt2. Activation of Slt2 by pheromone requires the polarisome component Spa2, which acts as scaffold for Mkk1 and Slt2. Deletion of the *SLT2* gene causes cell lysis during shmooing (7, 8).

An increase in external osmolarity causes loss of turgor pressure and cell volume, triggering a homeostatic response leading to accumulation of glycerol, which acts as the compensating osmolyte and to which the plasma membrane is only slightly permeable (10). The response also includes a temporary cell cycle arrest, changes in enzyme and transporter activities and stimulation of gene expression (1), responses that are mediated by the HOG system. The two signaling branches, Sln1 and Sho1, converge on the activation of the MAPKK Pbs2, which phosphorylates the p38 like MAPK Hog1 (11). Activation of the Sho1 branch by the mucin-like sensors Msb2 and Hrk1 causes the recruitment of Cdc42 to the membrane anchor Opy2, leading to activation of Ste20, which activates Ste11. Subsequently, Sho1 and the Opy2-Ste50 complex recruits Pbs2, enabling Ste11 to phosphorylate Pbs2 (12). The Sln1 branch transduces the signal through a phosphorelay signaling module, Sln1-Ypd1-Ssk1. In the absence of hyperosmotic stress, Sln1 is active, maintaining Ssk1 in its phosphorylated form. Following a hyperosmotic shock Sln1 activity decreases, leading to dephosphorylation of Ssk1. Unphosphorylated Ssk1 activates the MAPKKKs Ssk2 and Ssk22 (13), which phosphorylate Pbs2. Phosphorylated Hog1 translocates to the nucleus where it associates with transcription factors like Hot1 (14) and participates in the induction of various genes (15), including those encoding enzymes and transporters required for glycerol accumulation (1).

Osmotic shock also triggers HOG independent responses, such as rapid closure of the aquaglyceroporin Fps1 (16). Glycerol efflux through Fps1 occurs continuously in cells

growing in low osmolarity medium, but stops after osmotic shock and remains low after cells have adapted. When adapted cells are transferred into a low osmolarity environment, Fps1 opens, resulting in glycerol efflux and alleviating excessive pressure (16). Proper control of Fps1 activity seems to require two proteins, Rgc1 and Ask10, without which defects in Fps1 opening result in excessive accumulation of glycerol leading to cell wall stress (17).

Despite their similar core architecture consisting of two scaffolded-MAPK cascades, the PR and HOG display substantially different dynamic responses to constant stimulation. Exposure to a constant high pheromone concentration results in sustained gene induction and prolonged cell cycle arrest (5, 18). In contrast, a hyperosmotic shock causes a transient HOG activation followed by a slower deactivation phase as cells adapt (1). After adaptation, HOG is thought to return to its pre-shock state (11, 19, 20). This “perfect adaptation” implies that cells maintain a higher intracellular glycerol concentration (21) without the need for further HOG activity. Although the Sho1 branch of HOG shares components with PR (Fig. 1A), activation of each pathway does not cause activation of the other (22–24). PR is insulated from crossactivation by high-osmolarity through an unknown, cytoplasmic mechanism that requires Hog1 (23, 25).

Here, we examined the activity of HOG and its insulation from PR after adaptation to high osmolarity. We found that contrary to a previous report (19), HOG activity persists after adaptation in a dose-dependent manner. Unexpectedly, in osmo-adapted cells, PR activates HOG. This activation is not due to loss of insulation but to glycerol release caused by “shmooing”. HOG activation results in a state of high glycerol turnover that improves adaptability to rapid changes in osmolarity during mating. Our results illustrate the interplay between three MAPK pathways to mediate a cell shape change in the presence of external stress.

RESULTS

HOG remains active after adaptation to a hyperosmotic shock

To study the interaction between the PR and the HOG systems we constructed haploid *MAT*a strains that contained three fluorescent protein-based transcriptional reporters: P_{PRM1}-mCherry, which is induced by pheromone (26), P_{STL1}-YFP, which is induced by HOG (15) and P_{BMH2}-CFP, which is constitutively expressed and insensitive to either pathway (27) (Fig. 1A). To accurately control external pheromone concentration we used Δ*bar1* strains, which lack the extracellular protease Bar1. We applied pheromone or high osmolarity (NaCl, sorbitol, glycerol, or equal amounts of the last two compounds) and measured YFP, CFP and mCherry fluorescence by microscopy-based cytometry (28, 29).

As expected, each input activated only one reporter (Fig. 1B and C) (5, 15). Pheromone caused a steady, roughly linear accumulation of mCherry. Considering that degradation of these fluorescent proteins is negligible (27), and that cells are arrested by pheromone, the linear increase indicates that the expression of this reporter is constant, and suggests that the system is in steady state (27). High osmolarity caused a fast increase in YFP fluorescence followed by a slower decline. In cells adapted after overnight growth in high osmolarity medium, the steady state HOG transcriptional output did not return to pre-shock values, but instead, the output remained higher, in direct proportion to the external osmolarity (Fig. 2A). Expression of the constitutive P_{BMH2}-CFP reporter was not significantly affected by external osmolarity (Fig. S1A). The positive correlation between external osmolarity and steady-state activity of HOG suggests that Hog1 is required to maintain an increased internal concentration of glycerol during growth in high external osmolarities. At the same time, the chemical gradient across the membrane resulting from the increased internal glycerol

concentration drives glycerol out of cells, which can be compensated by a higher synthesis rate. To test if HOG was necessary to maintain a high internal glycerol concentration, we determined if its activity depends on the strength of the glycerol gradient. We compared reporter expression in cells grown in the presence of 1 M sorbitol or with 0.5 M sorbitol and 0.5 M glycerol. These two media present a similar osmotic challenge (30). However, in the second solution yeast experience a lower glycerol gradient and expression of the HOG reporter was lower than in 1 M sorbitol, adopting a value intermediate between 1 M glycerol and 1 M sorbitol (Fig. 2A). Hence, expression of the HOG reporter in steady state cultures depends on the glycerol gradient rather than on the absolute external osmolarity, supporting the notion that HOG activity in these cultures is directed at maintaining internal glycerol concentrations.

To confirm that HOG was active after osmoadaptation, we measured phosphorylated Hog1, total Hog1 and Hog1 subcellular localization in cells cultured overnight at different osmotic strength. Phosphorylated Hog1 increased proportionally with external osmolarity (Fig. 2B). This increase was due in part to an increase in total Hog1, especially at osmotic strengths higher than 1 Osm. In cells adapted to 1 M sorbitol, phosphorylation of Hog1 was similar to that observed after 5 minutes of osmoshock with 0.1 M NaCl (Fig. S1B). Also, the amount of nuclear Hog1 in adapted cells increased with osmolarity (Fig. 2C and Fig. S2) and exhibited large cell to cell variability (Fig. S3). The fluorescence of cytoplasmic Hog1-venus increased to a lesser extent than that of nuclear Hog1. Taken together, and in contrast to the “perfect adaptation” concept (19), it appears that HOG remains active after osmoadaptation.

To examine the effect of osmoadaptation on the activity of the pheromone pathway we measured pheromone dependent gene expression in cells grown at different osmotic strengths and stimulated with mating pheromone. Increased osmolarity resulted in decreased pheromone-dependent transcription (Fig. 2D) (for example, about 65% in medium with 1.6 M sorbitol compared to unstressed cells). Pheromone-induced cell cycle arrest was monitored by a halo assay, in which the size of the “halo” indicates the area of growth inhibition and the sensitivity of the cells to α factor. Cells spread on plates with 1 M sorbitol or mannitol formed smaller halos than cells spread on medium without added osmoticum (about 72% and 65% shorter diameter, respectively), whereas cells spread on plates with 1 M glycerol formed halos of normal size (Fig. 2E). Thus, when cells need to maintain the HOG system in an active state, the pheromone response is partly inhibited. This is consistent with reports that show that hyperosmolarity dampens the mating response (24, 31).

PR activates HOG

Whereas steady state HOG activity inhibited the pheromone pathway, pheromone further stimulated the HOG system. When cells pre-adapted to sorbitol were stimulated with pheromone, the expression of the HOG transcriptional reporter P_{STL1}-YFP began to increase after about 50 minutes (Fig. 3A) and was delayed compared to the PR reporter (Fig. S4A). Consistent with the increase in transcriptional activity, the amount of dually phosphorylated MAPK Hog1 (Fig. 3B) and of nuclear Hog1 (Fig. 3C) also increased. HOG reporter gene expression under these conditions was dependent on Hog1 because its activity was negligible in pheromone-stimulated, high-osmolarity-adapted Δ*hog1* cells (Fig. S5).

To demonstrate the involvement of the PR MAPK cascade in pheromone-dependent HOG activation, the experiment was repeated in Δ*fus3* cells. Induction of the HOG reporter, as well as the increase in Hog1 dual phosphorylation, were diminished (Fig. S6A and S14 and Table S1). Although the PR and the Sho1 branch of the HOG system share components (Fig. 1), deletion of the Sln1 branch components *SSK1* or *SSK2* but not of *SHO1* blocked reporter gene induction (Fig. 3A) as well as phosphorylation of Hog1 in response to

pheromone (Fig. S14 and Table S1). Hence, only the Sln1 branch mediates pheromone-dependent activation of HOG (Fig. 3D).

We next determined whether activation of HOG by PR takes place during mating. We mixed *MAT*a reporter strains with *MAT*α cells, both pre-adapted to growth in high osmolarity. As with synthetic pheromone, the HOG reporter P_{STL1}-YFP in the *MAT*a strain showed increased activity (Fig. S7). Taken together, these results suggest that during mating in high osmolarity environments, the PR, through the Sln1 branch, activates HOG.

PR activates HOG in bursts

In response to pheromone, average HOG reporter activity increased at a constant rate like that of the PR reporter (Fig. 3A and Fig. S4). However, at single cell level, the two reporters behaved differently. Whereas cells induced the PR reporter steadily over time (Fig. 4A), the HOG reporter was regulated in a seemingly stochastic manner (Fig. 4B). In addition, the activity of these two reporters was not substantially correlated (Fig. S8).

To understand the mechanism of HOG activation, we identified cells with similar temporal expression patterns with an adapted hierarchical clustering approach (32). Individual cells were clustered in rows according to a similar P_{STL1}-YFP expression pattern over time (Fig. S9A), which revealed that reporter induction was not random and occurred in transient bursts that typically lasted around 60 min. Cells exhibited bursts early or relatively late after pheromone stimulation. In general, there was a continuous temporal variation, from early to late bursts (Fig. 4C). Moreover, some cells exhibited more than one burst, separated by a variable interval (Fig. S9B and S10).

PR activation of HOG coincides with shmooing

Inspection of individual time courses revealed that bursts in HOG activity usually occurred around the time a mating projection formed (shmooing) (Fig. 5A and Fig. S10 and S11). To analyze the overall population behavior, we calculated the time interval between the moment the shmoo was first evident and the peak in HOG reporter expression for each cell. We found a large distribution of intervals, with a mode of approximately 50 minutes (Fig. 5B). To further support the idea that HOG activation occurs after shmooing, we correlated the onset of this shape change with the entry of Hog1 to the nucleus during pheromone response and showed that pheromone induced Hog1 translocation tends to occur after shmoos have formed (Fig. 5C). This sequence of events, during which shmooing formation precedes HOG activation, suggested that the former might be necessary for the latter.

A requirement for shmooing in pheromone-dependent HOG activation would explain why cells do not activate HOG simultaneously, because cells reach the G1 cell cycle stage, when shmooing can occur, at different times after pheromone addition. The timing of entry into G1 correlated with the beginning of shmooing and the onset of HOG reporter expression (Fig. S11). Dependence of HOG activation on shmooing would also explain why some cells exhibit more than one activation burst: Cells continuously exposed to pheromone develop new mating projections periodically. Although all bursts of HOG activity coincided with the formation of a mating projection, not all mating projections were accompanied by a burst in HOG activity (Fig. S10 and S11).

We explored the possibility of a causal link between shmooing and HOG activation by testing if PR activation of HOG occurred exclusively in conditions that promote proper shmooing. The polarisome is a multi-protein complex required for this type of polarized cellular growth. Δ*spa2* and Δ*pea2* mutants lacking two polarisome components (6) responded normally to pheromone and grew in a polarized manner but did not form the narrow, pointy shmoos characteristic of wild-type cells (Fig. 6A and B). Addition of

pheromone to either of these mutants resulted in reduced HOG activation. We further investigated the dose-dependence of PR activation of HOG by exploiting the fact that the concentration of pheromone required for shmooing is larger than that required for full transcriptional induction of pheromone inducible genes (33, 34). Therefore, if HOG activation required shmooing, the induction of the HOG reporter (P_{STL1}-YFP) should also require more pheromone for activation than the PR reporter (P_{PRM1}-mCherry). Indeed, although maximum PR reporter expression required 10 nM pheromone, the HOG reporter required more than 30 nM. In addition, the dose response curves of HOG reporter and of the fraction of cells exhibiting pointy shmoos were not significantly different (Fig. 6B; for our shape classification criteria see Fig. S12 and S13). Taken together, the data indicate that pheromone-stimulated activation of HOG requires shmooing.

Activation of HOG by PR requires the cell wall integrity MAPK Slt2

The polarisome assists in activating the CWI MAPK cascade through the scaffold Spa2, which interacts and recruits to the shmoo tip Slt2 and its MAPKK Mkk1 (35). This process results in transient activation of Slt2 (Fig. 1) during shmooing (8). Because phosphorylation of Slt2 after pheromone addition occurred at around the same time as Hog1 phosphorylation (Fig. 3B, Fig. S4) we hypothesized that activated Slt2 could be the signal that connected PR to the activation of HOG during shmooing. When Δ*slt2* cells were adapted to high osmolarity and treated with pheromone they formed normal shmoos but failed to activate HOG (Fig. 6A), indicating that morphogenesis is not sufficient to activate HOG and that Slt2 plays a critical role in this process. It also suggested that failure to activate Slt2 is the reason for the lack of activation of HOG in Δ*spa2* cells. Consistent with this notion, phosphorylation of Slt2 was reduced in the polarisome mutants Δ*spa2* and Δ*pea2* as compared to wild-type (Fig. S14).

PR activates HOG by blocking a homeostatic negative feedback

The intracellular glycerol concentration is determined by the rates of synthesis, degradation and efflux. Glycerol efflux occurs through the aquaglyceroporin Fps1, which has been implicated in cell fusion during mating (36). We speculated that pheromone might cause a rapid increase in glycerol efflux thereby leading to a burst in HOG activity (Fig. 7A).

Consistent with this idea, the extracellular glycerol concentration per cell increased to a greater extent in supernatants of cells treated with pheromone than in those of control cells (Fig. 7B). To determine if the release of glycerol was necessary for HOG activation, we reduced the chemical gradient of glycerol by using glycerol instead of sorbitol as the osmoticum. In this condition, pheromone treatment failed to activate HOG (Fig. 7C). Moreover, in cells with diminished plasma membrane permeability for glycerol (deletion mutants for *FPS1* or either *RGC1* or *ASK10*, which encode proteins required for Fps1 opening (17)) pheromone did not activate HOG (Fig. 7D). We further surmised that in cells adapted to osmolarities higher than 1M sorbitol, because they need to accumulate more glycerol, pheromone treatment would lead to a larger outward flux of glycerol. Under these conditions, cells would compensate for glycerol loss by more strongly activating HOG. Indeed, PR-mediated activation of HOG increased with increasing concentrations of extracellular sorbitol (Fig. 7E). These experiments indicate that pheromone-stimulated glycerol loss through Fps1 is necessary for the activation of HOG.

We also monitored phosphorylation of Hog1 by western blot in mutants with reduced reporter activity. Strains that showed reduced activation of the HOG transcriptional reporter in response to pheromone (*Δrgc1, Δask10, ΔrgcI Δask10, Δfps1, Δfus3, Δssk1, Δssk2, Δslt2, Δpea2* and *Δspa2)* also showed less increase in phosphorylation of Hog1 (Fig. S14 and Table S1). In contrast, these strains displayed a normal ability to activate HOG in

response to a hyperosmotic shock (Fig. S16), indicating that these proteins are specifically involved in PR activation of HOG. Finally, we tested if these strains failed to activate HOG due to a defect in the PR system itself. However, expression of the pheromone response reporter P_{PRM1}-mCherry was similar in all mutants to wild-type, except for *Δfus3*, which lacks the main MAPK of the PR (Fig. S6 and S14).

Pheromone activation of HOG facilitates acute response to high osmolarity shock

Pheromone-mediated activation of glycerol efflux appears to lead to a new steady state in which cells maintain their intracellular concentration of glycerol by compensating for glycerol loss with increased rate of production (Fig. 8A). Such regulation provides for faster turnover, enabling systems to adapt faster to changing signals (Fig. 8B) (37). Thus, we hypothesized that pheromone treated osmo-adapted cells might respond faster to further hyperosmotic stress. To test this idea, we shocked yeast adapted to sorbitol and pre-treated with pheromone, with NaCl (Fig. 8C) (28, 29) and monitored their change in volume over time. Indeed, pheromone treated cells recovered twice as fast as untreated cells (Fig. 8D, left), although cells in both populations lost the same fraction of their initial volume after the NaCl shock. In contrast, Δ*rgc1* cells, which cannot induce HOG in response to pheromone (Fig. 7D), recovered their original volume at the same speed independently of pheromone treatment and comparably to untreated wild-type cells (Fig. 8D). Similarly, control cells grown without osmoticum recovered from a 0.65 M NaCl shock only slightly faster when pretreated with pheromone (Fig. S17). Taken together, these results indicate that pheromone treatment results in an enhanced ability of cells to respond to osmotic shock.

DISCUSSION

We report a link between the pheromone and the high osmolarity response: In cells adapted to high osmolarity pheromone leads to HOG activation. We demonstrate that this effect is not due to direct crosstalk but rather to pheromone-induced drop in turgor pressure, which in turn is caused by glycerol release, probably mediated by the MAPK Slt2. Consequently, a discrete morphogenetic event links all four yeast MAP kinases: Fus3 and Kss1 as part of the pheromone pathway as well as periodic activation of Slt2 (8) and Hog1 (this work) by the morphogenetic changes induced by pheromone. Throughout the process all MAPKs maintain proper responsiveness to their canonical stimulus.

A previous study did not detect the link between PR and HOG (24). The discrepancy might be due to differences in experimental design, such as culture density. We have observed that PR activation of HOG is sensitive to this variable. In addition, we monitored HOG output at later time points and at higher external osmolarity. In fact, in one of the experiments reported by Patterson *et al.* (24), HOG output seems to be higher in the co-stimulated sample, suggesting HOG activation by PR actually occurs in this experiment.

The PR and HOG systems have been reported to inhibit each other (38), but we and others (24) have not been able to reproduce those results. In contrast, we detected a mild dampening of the PR pathway by high osmolarity, consistent with another report (31). This diminished PR output may be due to Hog1 mediated inhibition of Ste50 (31).

Increased glycerol release may have several functions

We report here that pheromone stimulation of osmo-adapted cells leads to a steady state with higher glycerol turnover. Such cells are able to adjust faster to changes in external osmolarity: Faced with a new osmotic shock, pheromone treated cells recovered twice as fast than untreated cells. Such an advantage may justify the energy invested in seemingly futile cycles of synthesis and degradation or loss.

In general, the increased glycerol turnover should help cells to control turgor faster and more precisely through the opening and closing of Fps1. Fast and precise turgor control maybe important specifically during mating. In support of this view, inability to control the osmotic balance in Δ*fps1* cells prevents mating at the prezygote step prior to cell wall degradation (36).

There could be additional roles for the increased release of glycerol induced by pheromone. For example, altered medium viscosity caused by glycerol might affect the shape of the pheromone gradient. Also the role of glycerol efflux in redox regulation may be relevant: Cells exposed to high pheromone concentrations produce increased amounts of reactive oxygen species (ROS) (39). High glycerol turnover provides an alternative path to mitochondrial re-oxidation of NADH, thus helping to reduce mitochondrial ROS production during mating. Consistent with this notion, cells with a deficient CWI pathway, which cannot activate HOG and thus are unable to increase the rate of glycerol turnover, produce increased ROS concentrations (39).

A cascade of MAPK cascades controls glycerol turnover rate

Mutations that prevent shmooing or that disrupt the CWI pathway greatly reduce pheromone-mediated HOG activation in osmo-adapted cells. Because CWI is activated by shmooing, a straightforward interpretation is that HOG activation by PR is caused by the PR-stimulated CWI. This leads to the hypothesis that CWI might stimulate Fps1-mediated glycerol release, which causes HOG activation in order to compensate turgor loss. Because both CWI and Fps1 are required for adaptation to hypo-osmotic shock it appears reasonable to propose that CWI controls Fps1-mediated glycerol release, although there is no experimental evidence to support it. In fact, deletion of *SLT2* and *FPS1* cause synthetic lethality, which has been interpreted as genetic evidence that these two gene products act in parallel (36, 40). On the other hand, *slt2* mutants display a weaker cell wall, which, in combination with a defect in glycerol release explains the observed hyper-fragility of the *slt2 fps1* double mutant, without excluding a direct regulation of Fps1 by Slt2. Here we report a condition in which the CWI pathway is required to activate HOG. Cell wall stress has been previously reported to activate the CWI pathway in a HOG-dependent manner through an osmolarity-independent mechanism that utilizes the Sho1 branch of HOG (41).

The HOG pathway remains active after osmoadaptation

Our work highlights a role for HOG activity during growth under high osmolarity. The glycerol production machinery has been postulated to have “memory” (19): HOG sets glycerol production to a desired amount during the acute response, which is later maintained without further HOG activity. In a continuously dividing cell population this does not seem to be the case. Our findings suggest that although HOG activity peaks and declines after an osmolarity increase, HOG activity is sustained at an osmolaritydependent amount to maintain appropriate glycerol accumulation. Thus, the dynamics of HOG does not display “perfect adaptation”. The need for a sustained osmolarity-dependent activity of HOG appears logical. When cell volume increases during growth, glycerol-producing enzymes would become diluted unless their synthesis matches the rate of volume change. It seems reasonable that HOG activity is continually required to maintain a high capacity for glycerol production with enhanced steady-state abundance of the enzymes involved (42, 43).

Not every shmoo results in a burst of HOG activity

Although PR-mediated HOG activation always coincides with mating projection formation, not all projections, even those of the same cell, lead to induction of the HOG transcriptional reporter (Fig. 5A, Fig. S10 and S11). This behavior could be due to stochastic transitions in the state of the chromatin at the loci inducible by Hog1 activity (44). Such stochastic effects

are more evident when cells are exposed to mild osmostress and indeed the extent of Hog1 phosphorylation achieved following pheromone treatment is similar to a mild osmoshock (100 mM NaCl) (Fig. S1B). Hence HOG activity might burst in every cell during every shmoo but this activity might not always be translated into enhanced gene expression, our experimental output. As an alternative explanation, glycerol might be released only during some of the shmooing events. We have previously shown that the activity of the PR system displays large cell to cell variation (27). Given our findings that activation of HOG requires activation of two MAPK cascades, it is conceivable that cell-to-cell differences in the activity of components necessary for HOG activation result in some cells being unable to release glycerol.

Definition of pathways depends on context

A signaling pathway is commonly defined by a specific stimulus resulting in a distinct output. This experimental definition may not hold for many natural conditions. For instance, activation of the HOG pathway is not an output triggered by pheromone under low osmolarity conditions. However, low osmolarity might not necessarily be a normal condition for yeast. Yeast thrives in environments with high sugar concentrations that constitute a high osmolarity condition, such as grape juice, which has an osmolarity around 1 Osm (45), similar to the experimental conditions used in this study. Consequently, in such a condition activation of the HOG pathway appears to be a normal output for the stimulus pheromone. Thus, in “real life” classically defined pathways might operate in a far more flexible manner, employing different connectivity depending on context.

Integration of signals in eukaryotic cells expands pathway’s functions

As with yeast PR and HOG systems, which respond to different types of signals (developmental and stress), many apparently independent signaling pathways in eukaryotic cells might have evolved mechanisms of interaction. These mechanisms might only become apparent in the appropriate signaling context. The consequence of the activation of one system by another is to bring about different functional properties to the overall behavior. In the case presented here, the HOG system enables volume control during mating response. This type of interaction is likely to be common in multicellular eukaryotes, both in normal and pathological conditions. For example, growth factors and morphogens drive cellular and tissue differentiation, often involving cell shape changes, as well as changes in cell-cell and cell-matrix interactions. In turn, these mechanical stresses activate pathways that shape the response to the growth signal (46, 47). Similarly, miss-regulation of this interplay between mechano- and growth factor-initiated signaling might enhance cancer progression (48, 49). Such multiple signals modulate one another, resulting in system level behaviors that are hard to guess a priori. Understanding the nature and consequences of these interactions might help design new strategies that block (or enhance) the ability of one pathway to recruit another.

Materials and Methods

Genetic and Molecular Biological Methods

Nucleic acid and yeast manipulations were performed as described (50, 51).

Yeast Strains

Strains are detailed in Table S2. ACL379 was used as the parental strain, which is a Δ*bar1* strain derived from YAS245-5C (*can1::HO-CAN1 ho::HO-ADE2 ura3 ade2 leu2 trp1 his3*), which in turn is a W303-1a descendant (27).

LD3342 was constructed in three steps. First, we transformed ACL379 with plasmid pRS406-P*STL1*-YFP, which bears the HOG inducible reporter *STL1*. The plasmid was linearized with AflII within the *STL1* promoter, transformed into yeast and transformants were selected for uracil prototrophy. To make ACL3341, we replaced the *PRM1* ORF, a pheromone inducible gene, with mCherry. Replacement was achieved by homologous recombination using a PCR product containing mCherry followed by a hygromycin resistance cassette, flanked by 40 nucleotides of homology with the borders of *PRM1* coding sequence. In a third step, we obtained LD3342 by transforming ACL3341 with plasmid pBMH2-CFP-404 linearized within the *BMH2* promoter using NdeI, and selecting transformants for uracil and tryptophan prototrophy. The resulting strain expressed CFP constitutively and maintained inducibility of YFP and mCherry.

Plasmids

pRS404-P*STL1*-CFP and pRS406-P*STL1*-YFP were constructed as follows. As backbone, we used pTC414-CFP and pTC416-YFP (27), which are derivatives of pRS414 and pRS416 (58) and contain the CEN-ARS region flanked by AatII sites. pTC414-CFP and pTC416-YFP contain the *GAL1* promoter cloned between Acc65I and EcoRI driving the expression of CFP or YFP, respectively. pTC414-CFP and pTC416-YFP were cut with Acc65I and EcoRI and the backbone was gel-purified from the *GAL1* promoter. In parallel, we PCR amplified the *STL1* promoter region (−950 to −1 with respect to the START codon) using primers 5' STL1p (ctcggaattaaccctcactaaagggaacaaaagctgggtaccCAGTCTGATATTACGAGCGAC) and 3'STL1p (cagtgaaaagttcttctcctttactcatggatccgaattcGGTCTAAAACTTTCTATGTTCTA) and yeast genomic DNA as template. These primers contain a 40 nt tail (denoted by the lowercase letters) homologous to the ends of the purified backbone of pTC414-CFP and pTC416-YFP. The PCR product with the *STL1* promoter was co-transformed with either of the cut backbones into the ACL379 yeast strain (27), and colonies were selected on SC-TRP or SC-URA plates. Plasmids were recovered from colonies that expressed CFP or YFP in 1 M NaCl SC medium. CEN-ARS from these plasmids were removed by digestion with AatII, and religated to create pRS404- P*STL1*-CFP and pRS406- P*STL1*-YFP. pRS404- P*STL1*-CFP or pRS406- P*STL1*-YFP were used to integrate the *STL1* promoter driving CFP or YFP, at the *TRP*1 and *URA3* locus respectively. pP*BMH2*-CFP-TRP1 was used to integrate the P*BMH2*-CFP construct at the *BMH2* locus (27). *fps1*Δ*::HIS3*-long was used to delete *FPS1* (42).

Single Cell Microscopy Methods—Cultures were maintained in exponential growth for at least 15 h. We typically inoculated two or three cultures with different amount of cells to ensure that after overnight growth at 30°C with agitation, at least one of the cultures was at an optical density (OD) between 0.05–0.1. This low OD minimizes cellular autofluorescence, especially in the vacuole (27, 28, 52). In addition, we have observed that PR activation of the HOG reporter is reduced in cultures at ODs higher than 0.3.

For samples taken at different times from a liquid culture, cycloheximide was added to samples at a final concentration of 100 μg/ml and cells were incubated for at least 3 hours before imaging, which stops further translation but allows for full maturation of the reporter fluorescent proteins YFP, CFP and mCherry produced at each given time point (27).

For movies, cultures were sonicated to disperse clumps and 100 μl of cell suspension (roughly 10^6 cells) were applied to 96-well glass bottom plates that had been pre-coated with concanavalin A type V (Sigma-Aldrich; 10 μg per well). After allowing yeast to settle and attach for 10 min, unbound cells were washed off. At this point, we manually selected

three or more image fields per well, acquired time 0 images, replaced the medium with fresh medium containing α-factor (Sigma-Aldrich) and started time lapse imaging.

For imaging, a 60X PlanApo objective (N.A.=1.4) was used under oil immersion in a Olympus IX81 inverted microscope equipped with a mercury lamp, a motorized XYZ stage and a CoolSnapHQ2 cooled CCD camera (Photometrix, Tucson AZ) in a 30°C room. We automatically and repeatedly imaged multiple wells over time using MetaMorph 7.5 software (Universal Imaging Corporation, Downingtown, PA). MetaMorph was also used to control the built-in motorized XYZ-motor and cube changer.

To avoid non-specific binding of α factor to plastic, α factor was prepared in BSM (Q-Bio gene, MPBiomedicals, Santa Ana, CA) medium containing 20 μg/ml of casein as a blocking reagent (from the DIG nucleic acid detection kit, Roche Diagnostics Corporation, Indianapolis, IN). Blocking non-specific adsorption enabled reproducibility when performing experiments with low doses of α factor.

For each time and field, we acquired a bright field image and RFP, YFP and CFP fluorescence images using filter sets 41004, 31044v2 and 41028 from Chroma Technologies Corp. (Brattleboro, Vermont).

To extract quantitative information images were processed with VCell-ID as previously described (28, 29). Data extracted from VCell-ID were further analyzed using R (http://www.r-project.org) with VCell-ID specific analysis package Rcell (http://cran.r-project.org/web/packages/Rcell/index.html).

To calculate the transcriptional output of each pathway per cell (defined as the total corrected fluorescence signal in a cell from the corresponding reporter gene), the background signal measured outside the cells was subtracted from the integrated total fluorescence for a given cell (the sum of the fluorescence values of all the pixels that VCell-ID associated with that cell).

To quantify the nuclear localization of Hog1, images were acquired in an Olympus IX81 inverted microscope coupled to a spectral confocal module FV1000 (Olympus, Latin America) with a 60×1.35 NA oil immersion objective. Excitation and filters were as follows: for Hta2-CFP, 458 nm excitation, emission 470–510 nm; for Hog1-Quadruple-Venus, 515 nm excitation, emission 530–630 nm. Different channels were acquired sequentially in Kalman line filtering mode. The pinhole diameter was 300 μm. We acquired 6 Z slices with a step of 0.21 μm to obtain maximum fluorescence corresponding to the focal plane of the nucleus. Images were processed in VCell-ID and the fluorescent nuclear tag was specified as the CFP channel (29). We used the variables *f.nucl4.y* (quantifies the fluorescence of a disc with a radius of 5 pixels) and *a.nucl4.y* for the nuclear fluorescence and nuclear area, respectively. We used *f.tot.y* minus *f.nucl6.y* and *a.tot* minus *a.nucl6*, to estimate the fluorescence and the area of the cytoplasm, respectively. *f.tot.y* corresponds to the yellow fluorescence of all pixels inside the cell. *f.nucl6.y* measures the fluorescence inside in the total area of the nucleus in all cells analyzed (Figure S2). Because the equatorial planes of cells were at slightly different Z positions, resulting in different cells having their maximum fluorescence intensity in different Z slices, and because nuclei are not necessarily located at the equatorial plane of each cell, we used the function “append.in.focus” in the *Rcell* package for R, which generates a Boolean variable that is attached to each slice of a Z stack. This variable is TRUE only at the slice that presents the maximum value for a chosen VCell-ID variable. The function to the *f.nucl1.c* variable was applied to identify the slice where the nucleus is located for each individual cell.

To analyze a large number of cells for statistical analysis, seven different fields were sampled. Because the time courses were long we started the movies with a low number of cells in each field to avoid cells dividing and growing too close to each other. After VCell-ID processing we used Rcell to filter cells that were recognized with incorrect boundaries and cells that were not recognized in most of the time points of the movies. We preferred using YFP density variable because it is more robust to cell boundary artifacts. After filtering, 200 cells were analyzed.

Hierarchical clustering of the cells was performed using the software “Gene cluster 3.0” [http://bonsai.hgc.jp/~mdehoon/software/cluster/]. Cells were clustered using the following variable for each cell: $\frac{\Delta(\mathrm{YFPdensity})}{\Delta(\mathrm{time})}$, which corresponds to the change in the abundance of the HOG reporter from time “i” and time “i-1”.

Several similarity metrics and clustering methods were tested with the conclusion that the "centered correlation" metric clustered using the “average linkage” algorithm worked best to separate the different group of cells.

To determine the HOG bursts in single cell time courses, we calculated the time of YFP fluorescence increase (time of burst) by applying a local polynomial regression fitting (loess) (53) to the time dependent YFP fluorescence signal of each cell, calculating the time derivative of the smoothed traces, and selecting the local maxima of these derivatives as the time for a burst. The time of shmoo formation was manually annotated for a random subset of cells based on the transmission images. Every burst of YFP fluorescence was preceded by a shmoo formation. A histogram for the time between burst and the preceding shmoo is shown in Fig. 5B.

To quantify mating projection morphology, shape categories were assigned as shown in Supplementary Figure S12. A "shmoo" was defined as those cells presenting a sharp mating projection with concave curvatures in its base (category 1). The fraction of shmoos and the other morphologies was quantified using the ImageJ plug-in "cell counter". We provide the images with the labels used in the quantitation (Figure S13).

For volume recovery experiments, we acquired a Z-stack of eight slices of 0.4 μm covering 2 μm on either side of the focused image. Images were acquired for 10 minutes to quantify pre-shock volumes of the pheromone-stimulated or control cells. Cells were then stimulated by hyperosmotic-shock which resulted in a 30 second gap in the time-lapse. We then acquired images every minute for 100–120 minutes. For each Z stack, we selected the picture in focus as follows. The "Kurtosis coefficient" of the distribution of pixel intensities of bright field images calculated by ImageJ [http://rsbweb.nih.gov/ij/] shows a maximum at the slice of the bright field picture that is in focus. In addition, the standard deviation of this pixel distribution presents a minimum value in the picture that is in focus. Thus, we created a new variable in R called "kurtosis.focus" that is 0 (zero) for the image in focus (maximum kurtosis) and increases for images of slices above focus (for example, 1, 2, 3, and so on) and decreases for images below focus (for example, −1, −2, −3, and so on). The defocused images with kurtosis.focus equal to −3 were processed using VCell-ID. We used the VCell-ID variable sphere.vol to quantify cell volume.

Protein Methods—Samples were prepared using a modified protocol based on Yu *et al.* (52). For each time point, 5.0 ml of exponentially growing cells (OD ≤ 0.3) were mixed with 412.5 μl of 10M NaOH and 50 μl of 100% 2-mercaptoethanol (premixed immediately before the experiment). Samples were incubated at room temperature for at least 5 min, then 750 μl of 100% trichloroacetic acid (Sigma-Aldrich, St. Louis, MO) was added. We mixed and

incubated on ice for at least 10 min. We sedimented samples at 4,500 g for 30 min at 4 °C, aspirated the supernatant, added 700 µl of ice-cold acetone solution (70%v/v acetone in TrisHCl 100 mM, pH 6.8) and incubated for 5 min on ice. The pellet was sonicated for 20 s at 40% amplitude (Sonic Dismembrator, Fisher Scientific, USA), transferred to a microfuge tube and sedimented at >16000g for 2 min, aspirated and air-dried.

For protein quantitation samples were prepared by resuspending pellets in 40 µl of resuspension buffer (100 mM Tris pH 8.8, 3% SDS) at 65 °C for 30 minutes and in a disruptor genie (Scientific Industries, USA) for 2 min, followed by centrifugation for 10 min at >16000g (at 4 °C) to clear cellular debris before quantitation. Protein concentration was quantified using the BCA Protein Assay Kit (Pierce Cat# 23225).

After quantitation, protein solutions were mixed with an equal volume of SDS-PAGE loading buffer (10 mM Tris pH 6.8, 0.002% bromophenol blue, 100 mM dithiothreitol, 2% SDS, 50% glycerol), boiled for 5 min and loaded onto the electrophoresis gel.

Protein samples were separated using 12% Tris-HCl/glycine polyacrylamide gels (Bio-Rad, Hercules, CA), then transferred onto 0.2 µm Immobilon-FL PVDF membrane (IPFL00010, Millipore, Billerica, MA). Membranes were blocked for at least 1 h at room temperature in Tris-buffered saline (TBS, 10 mM Tris pH 7.4, 150 mM NaCl) plus 1/10th volume of Western Blocking Reagent (WBR) (Roche, Alameda, CA). Phosphorylated MAPKs Fus3, Kss1 and Mpk1/Slt2 were detected with rabbit anti-phosphoP44/P42 at 1:1000 dilution (Cell Signaling Technology, Danvers, MA, Catalogue #9101L). Hog1 was detected with mouse anti-phosphoP38 at 1:1000 dilution (Cell Signaling Technology, Danvers, MA, Catalogue #9216L), which detects only dually phosphorylated MAPK, in primary antibody binding buffer (TBS, 1/10th volume WBR, and 0.05% Tween). Total Hog1 was detected using anti-Hog1 (yC-20 SC-6815) at 1:5000 dilution (Santa Cruz. Biotechnology, Inc.). Gapdh was detected using a 1:10000 dilution of mouse anti-Gapdh antibody (Sigma Cat# A9521-1VL). Blots were washed in TBS with 0.05% Tween and probed for 1 h at room temperature with 800 nm donkey anti-rabbit (926-32213 IRDye® 800CW Donkey anti-Rabbit IgG (H + L), Li-Cor Biosciences), 800 nm donkey anti-mouse (926-32212 IRDye 800CW® Donkey anti-Mouse IgG (H + L), Li-Cor Biosciences) and 680 nm donkey anti-goat (926-68074 IRDye® 680RD Donkey anti-Goat IgG (H+L)) fluorophore-conjugated secondary antibodies (Invitrogen, Carlsbad, CA), diluted 1:15,000 in secondary antibody binding buffer (TBS, 1/20th volume WBR, 0.05% Tween). Blots were washed in TBS and then scanned on a LiCor infrared imaging system (Li-Cor Biosciences, Lincoln, NE). Band intensities were quantified using Odyssey ImageStudio software (Li-Cor Biosciences) employing median top/bottom background correction.

For some experiments we used peroxidase-labeled secondary antibodies (1/10000, Biorad), incubated for 1 h at room temperature in TBS with 1/20th volume WBR 0.05% Tween. After washing 3×10 min in TBS at room temperature, blots were developed using the Pierce SuperSignal ECL Western Blotting Detection Reagents (#34075) with a Luminiscence image analyser LAS-1000 (FujiFilm).

Glycerol measurements—Yeast cells were grown overnight in SC medium with 1 M sorbitol at 30 °C starting with an OD such that on the following day, the OD was 0.2. The culture was filtered (cellulose ester filtering discs of 0.45 µm pore size, 25mm de diameter - Millipore, USA, cat. number HAWP02500) in a "1225 manifold" (Millipore, USA, cat. number XX2702550) and resuspended in fresh medium. This step is necessary to remove glycerol produced prior to the experiment. Cells were divided into two cultures of 30 ml. One of these cultures was treated with 5 µM α factor. As a reference value for glycerol release, cells were subjected to a hypo-osmotic shock to induce release of glycerol (16) by

resuspending 6.5 ml of the filtered untreated culture in SC medium without sorbitol at 0, 100, 200 and 300 min of the time-course experiment. The samples were evaporated in a Speed-Vac for 30 min to remove ethanol, dialysis filtered with Amicom Ultra < 3 KDa (UFC500396-Millipore, USA) to remove high molecular weight compounds, and subjected to HPLC for glycerol quantification.

In the same experiments we collected samples at 0, 50, 100, 150, 200, 250 and 300 min, added cycloheximide to a final concentration of 100 μg/mL, measured OD, and imaged cells to quantify cell volume and reporter expression.

The concentration of glycerol was measured by high pH anion exchange chromatography with pulse amperometric detection (HPAEC-PAD) in an ICS-3000 chromatographic system, (DIONEX), as previously described (54). We used a CarboPac MA1 column (4×250mm, DIONEX) and a CarboPac MA1 guard column (4×50mm, DIONEX). An isocratic program with 200 mM NaOH was used at a flow rate of 0.5 ml/min and a loop of 20 μl. The standard curve was measured between 0 and 4000 ng of glycerol. Samples were diluted as necessary to obtain data in this range.

The following mathematical transformation was used to calculate the amount of glycerol produced per cell.

$$\left.\frac{\text{Glycerol(pmols)}}{\text{cell}}\right|_{\text{tx}} = \frac{[\text{Glycerol}]_{\text{tx}}(ng/\mu L)}{OD_{\text{tx}}} * \left.\left(\frac{OD{=}1}{3{*}10^{7}\,\text{cels}/mL}\right)\right|_{\text{Vrel}=1} * \text{Vrel}_{\text{tx}} * \left(\frac{10^{6}\mu L}{1mL}\right)$$

where $Vrel_{tx}$ is the relative volume of cells at a certain time (tx) relative to the volume of cells at time zero. In Figure S15 changes in cell number and cell volume over time are shown for these experiments.

Osmolarity determination—The osmolarity of all media was measured using a Vapro 5520 Osmometer (Wescor, inc.).

Halo assays—Halo assays were performed as previously described (50, 51). Briefly, 10^6 cells were plated on agar plates with different media: SC or SC supplemented with either sorbitol, mannitol and glycerol at several concentrations. After plating the cells a sterile disc of Whatman paper (5mm diameter) was placed in the middle of the Petri dish and 3 μL of 1 mM α factor were applied.

Statistical methods—Several statistical methods were used throughout this work. For the analysis of fluorescence transcriptional reporters (P_{STL1}-YFP, P_{PRM1}-mCherry), localization reporters (Hog1-Venus) and for the analysis of western blots data, linear mixed-effects models were fitted to the data using the *nlme* package for R (55). When analyzing the dependence of a response variable with a continuous covariate (namely time or osmolality), a polynomial model of adequate order was used. As examples, a cubic term was needed to fit the data of Fig. 2A and linear terms on the variables were required to fit the data of Fig. 2C. Random effects were used to explain systematic differences among repetitions of an experiment. For example, if three repetitions of a western blot were done in three independent gels, a random *gel effect* was used to account for gel-to-gel variations (that might derive from small differences in incubation times, antibody concentrations, etc.). This procedure reduces the unexplained variability and therefore increases the power of the analysis (55). Tukey´s multiple comparisons were implemented with the *multcomp* package for R when required. The quality of the fits was inspected visually by comparing the

predicted values with the measured data, and by looking at the distribution of the residuals. Models that account for heteroscedastic data were used when appropriate.

The dose response curves in Fig. 6B were independently fitted by nonlinear least squares to Hill functions, and the EC_{50} values compared based on the estimated values and standard errors.

To test if there was a significant correlation between the time of shmoo formation and the increase in nuclear Hog1-Venus (Fig. 5C), a permutation analysis was done. The integral of the nuclear Hog1-Venus to Hta2-CFP ratio after the time of shmoo was used as a statistic (region to the right of the dotted line in Fig. 5C). The distribution of the statistic under the null hypothesis was calculated by permutations of the time of shmoo formation between cells. Only 1 of the 10000 permutations resulted in a value greater than the one observed. Similar results are obtained with other statistics.

For the volume recovery experiments (Fig. 8D and Fig. S17), the volume as a function of time trace for each cell was smoothed using a loess regression (53) and the ET_{25} (effective time it takes each cell to recover 25% of the volume lost after the shock) was calculated. A mixed-effects model was fitted to the distribution of ET_{25}.

Supplementary Material

Refer to Web version on PubMed Central for supplementary material.

Acknowledgments

We are grateful to Gustavo Pesce for constant feedback and advice. We thank Serge Pelet (Matthias Peter lab), Gustavo Pesce, Rich Yu and Eduard Serra (Molecular Sciences Institute) for providing strains and plasmids. We also thank Sergi Regot (Francesc Posas lab), Raul Salcedo, Elzbieta Petelenz, Doryaneh Ahmadpour (Stefan Hohmann lab), Christian Waltermann (Edda Klipp lab) and Alberto Kornblihtt for helpful discussions. FUNDING: Work in the laboratory of SH was supported by the Swedish Research Council and the European Commission (UNICELLSYS, contract 201142). Work in the laboratory of ACL was supported by grants PICT2005-33624, PICT-2007-847 and PICT2010-2248 from the Argentine Agency of Research and Technology (ANPCyT) to ACL and grant 1R01GM097479-01, subaward 0000713502 from NIGMS-NIH.

REFERENCES AND NOTES

1. Hohmann S. Osmotic stress signaling and osmoadaptation in yeasts. Microbiol Mol Biol Rev. 2002; 66:300. [PubMed: 12040128]
2. Levin DE. Regulation of cell wall biogenesis in Saccharomyces cerevisiae: the cell wall integrity signaling pathway. Genetics. 2011; 189:1145. [PubMed: 22174182]
3. Dohlman HG, Thorner JW. Regulation of G protein-initiated signal transduction in yeast: Paradigms and Principles. Annu.Rev.Biochem. 2001; 70:703. [PubMed: 11395421]
4. Madhani HD, Fink GR. The control of filamentous differentiation and virulence in fungi. Trends Cell Biol. 1998; 8:348. [PubMed: 9728395]
5. Roberts CJ, Nelson B, Marton MJ, Stoughton R, Meyer MR, Bennett HA, He YD, Dai H, Walker WL, Hughes TR, Tyers M, Boone C, Friend SH. Signaling and circuitry of multiple MAPK pathways revealed by a matrix of global gene expression profiles. Science. 2000; 287:873. [PubMed: 10657304]
6. Chenevert J, Valtz N, Herskowitz I. Identification of genes required for normal pheromone-induced cell polarization in Saccharomyces cerevisiae. Genetics. 1994; 136:1287. [PubMed: 8013906]
7. Errede B, Cade RM, Yashar BM, Kamada Y, Levin DE, Irie K, Matsumoto K. Dynamics and organization of MAP kinase signal pathways. Mol.Reprod.Dev. 1995; 42:477. [PubMed: 8607979]
8. Buehrer BM, Errede B. Coordination of the mating and cell integrity mitogen-activated protein kinase pathways in Saccharomyces cerevisiae. Mol.Cell Biol. 1997; 17:6517. [PubMed: 9343415]

9. Zarzov P, Mazzoni C, Mann C. The SLT2(MPK1) MAP kinase is activated during periods of polarized cell growth in yeast. Embo J. 1996; 15:83. [PubMed: 8598209]
10. Sutherland FC, Lages F, Lucas C, Luyten K, Albertyn J, Hohmann S, Prior BA, Kilian SG. Characteristics of Fps1-dependent and -independent glycerol transport in Saccharomyces cerevisiae. J Bacteriol. 1997; 179:7790. [PubMed: 9401039]
11. de Nadal E, Ammerer G, Posas F. Controlling gene expression in response to stress. Nat Rev Genet. 2011; 12:833. [PubMed: 22048664]
12. Yamamoto K, Tatebayashi K, Tanaka K, Saito H. Dynamic control of yeast MAP kinase network by induced association and dissociation between the Ste50 scaffold and the Opy2 membrane anchor. Mol Cell. 2010; 40:87. [PubMed: 20932477]
13. Posas F, Saito H. Activation of the yeast SSK2 MAP kinase kinase kinase by the SSK1 two-component response regulator. Embo J. 1998; 17:1385. [PubMed: 9482735]
14. Ferrigno P, Posas F, Koepp D, Saito H, Silver PA. Regulated nucleo/cytoplasmic exchange of HOG1 MAPK requires the importin beta homologs NMD5 and XPO1. EMBO J. 1998; 17:5606. [PubMed: 9755161]
15. O'Rourke SM, Herskowitz I. Unique and redundant roles for HOG MAPK pathway components as revealed by whole-genome expression analysis. Mol Biol Cell. 2004; 15:532. [PubMed: 14595107]
16. Luyten K, Albertyn J, Skibbe WF, Prior BA, Ramos J, Thevelein JM, Hohmann S. Fps1, a yeast member of the MIP family of channel proteins, is a facilitator for glycerol uptake and efflux and is inactive under osmotic stress. Embo J. 1995; 14:1360. [PubMed: 7729414]
17. Beese SE, Negishi T, Levin DE. Identification of positive regulators of the yeast fps1 glycerol channel. PLoS Genet. 2009; 5:e1000738. [PubMed: 19956799]
18. Moore SA. Alpha-factor inhibition of the rate of cell passage through the "start" step of cell division in Saccharomyces cerevisiae yeast: estimation of the division delay per alphafactor.receptor complex. Exp Cell Res. 1987; 171:411. [PubMed: 3040450]
19. Muzzey D, Gomez-Uribe CA, Mettetal JT, van Oudenaarden A. A systems-level analysis of perfect adaptation in yeast osmoregulation. Cell. 2009; 138:160. [PubMed: 19596242]
20. Miermont A, Uhlendorf J, McClean M, Hersen P. The Dynamical Systems Properties of the HOG Signaling Cascade. Journal of signal transduction. 2011:930940. [PubMed: 21637384]
21. Oliveira R, Lucas C. Expression studies of GUP1 and GUP2, genes involved in glycerol active transport in Saccharomyces cerevisiae, using semi-quantitative RT-PCR. Curr Genet. 2004; 46:140. [PubMed: 15278288]
22. Posas F, Saito H. Osmotic activation of the HOG MAPK pathway via Ste11p MAPKKK: scaffold role of Pbs2p MAPKK. Science. 1997; 276:1702. [PubMed: 9180081]
23. O'Rourke SM, Herskowitz I. The Hog1 MAPK prevents cross talk between the HOG and pheromone response MAPK pathways in Saccharomyces cerevisiae. Genes Dev. 1998; 12:2874. [PubMed: 9744864]
24. Patterson JC, Klimenko ES, Thorner J. Single-Cell Analysis Reveals That Insulation Maintains Signaling Specificity Between Two Yeast MAPK Pathways with Common Components. Sci. Signal. 2010; 3 ra75.
25. Westfall PJ, Patterson JC, Chen RE, Thorner J. Stress resistance and signal fidelity independent of nuclear MAPK function. Proc Natl Acad Sci U S A. 2008; 105:12212. [PubMed: 18719124]
26. Heiman MG, Walter P. Prm1p, a pheromone-regulated multispanning membrane protein, facilitates plasma membrane fusion during yeast mating. J Cell Biol. 2000; 151:719. [PubMed: 11062271]
27. Colman-Lerner A, Gordon A, Serra E, Chin T, Resnekov O, Endy D, Pesce CG, Brent R. Regulated cell-to-cell variation in a cell-fate decision system. Nature. 2005; 437:699. [PubMed: 16170311]
28. Gordon A, Colman-Lerner A, Chin TE, Benjamin KR, Yu RC, Brent R. Single-cell quantification of molecules and rates using open-source microscope-based cytometry. Nat Methods. 2007; 4:175. [PubMed: 17237792]

29. Chernomoretz A, Bush A, Yu R, Gordon A, Colman-Lerner A. Using Cell-ID 1.4 with R for microscope-based cytometry. Current protocols in molecular biology / edited by Frederick M. Ausubel … et al. 2008; Chapter 14:18. Unit 14. [PubMed: 18972382]
30. Karlgren S, Pettersson N, Nordlander B, Mathai JC, Brodsky JL, Zeidel ML, Bill RM, Hohmann S. Conditional osmotic stress in yeast: a system to study transport through aquaglyceroporins and osmostress signaling. J Biol Chem. 2005; 280:7186. [PubMed: 15611083]
31. Nagiec MJ, Dohlman HG. Checkpoints in a Yeast Differentiation Pathway Coordinate Signaling during Hyperosmotic Stress. PLoS Genet. 2012; 8:e1002437. [PubMed: 22242015]
32. Eisen MB, Spellman PT, Brown PO, Botstein D. Cluster analysis and display of genome-wide expression patterns. Proc.Natl.Acad.Sci.U.S.A. 1998; 95:14863. [PubMed: 9843981]
33. Moore SA. Comparison of dose-response curves for alpha factor-induced cell division arrest, agglutination, and projection formation of yeast cells. Implication for the mechanism of alpha factor action. J.Biol.Chem. 1983; 258:13849. [PubMed: 6358212]
34. Dorer R, Pryciak PM, Hartwell LH. Saccharomyces cerevisiae cells execute a default pathway to select a mate in the absence of pheromone gradients. J.Cell Biol. 1995; 131:845. [PubMed: 7490289]
35. van Drogen F, Peter M. Spa2p functions as a scaffold-like protein to recruit the Mpk1p MAP kinase module to sites of polarized growth. Curr Biol. 2002; 12:1698. [PubMed: 12361575]
36. Philips J, Herskowitz I. Osmotic balance regulates cell fusion during mating in Saccharomyces cerevisiae. J.Cell Biol. 1997; 138:961. [PubMed: 9281576]
37. Alon, U. An Introduction to Systems Biology: Design Principles of Biological Circuits (Chapman & Hall/CRC Mathematical & Computational Biology). Chapman & Hall; 2006.
38. McClean MN, Mody A, Broach JR, Ramanathan S. Cross-talk and decision making in MAP kinase pathways. Nat Genet. 2007; 39:409. [PubMed: 17259986]
39. Zhang NN, Dudgeon DD, Paliwal S, Levchenko A, Grote E, Cunningham KW. Multiple signaling pathways regulate yeast cell death during the response to mating pheromones. Mol Biol Cell. 2006; 17:3409. [PubMed: 16738305]
40. Tamas MJ, Luyten K, Sutherland FC, Hernandez A, Albertyn J, Valadi H, Li H, Prior BA, Kilian SG, Ramos J, Gustafsson L, Thevelein JM, Hohmann S. Fps1p controls the accumulation and release of the compatible solute glycerol in yeast osmoregulation. Mol Microbiol. 1999; 31:1087. [PubMed: 10096077]
41. Rodriguez-Pena JM, Garcia R, Nombela C, Arroyo J. The high-osmolarity glycerol (HOG) and cell wall integrity (CWI) signalling pathways interplay: a yeast dialogue between MAPK routes. Yeast. 2010; 27:495. [PubMed: 20641030]
42. Rep M, Albertyn J, Thevelein JM, Prior BA, Hohmann S. Different signalling pathways contribute to the control of GPD1 gene expression by osmotic stress in Saccharomyces cerevisiae. Microbiology. 1999; 145(Pt 3):715. [PubMed: 10217506]
43. Klipp E, Nordlander B, Kruger R, Gennemark P, Hohmann S. Integrative model of the response of yeast to osmotic shock. Nat Biotechnol. 2005; 23:975. [PubMed: 16025103]
44. Pelet S, Rudolf F, Nadal-Ribelles M, de Nadal E, Posas F, Peter M. Transient activation of the HOG MAPK pathway regulates bimodal gene expression. Science. 2011; 332:732. [PubMed: 21551064]
45. Wendland BE, Arbus GS. Oral fluid therapy: sodium and potassium content and osmolality of some commercial "clear" soups, juices and beverages. Canadian Medical Association journal. 1979; 121:564. [PubMed: 497946]
46. Streuli CH, Akhtar N. Signal co-operation between integrins and other receptor systems. Biochem J. 2009; 418:491. [PubMed: 19228122]
47. Bill HM, Knudsen B, Moores SL, Muthuswamy SK, Rao VR, Brugge JS, Miranti CK. Epidermal growth factor receptor-dependent regulation of integrin-mediated signaling and cell cycle entry in epithelial cells. Mol Cell Biol. 2004; 24:8586. [PubMed: 15367678]
48. Butcher DT, Alliston T, Weaver VM. A tense situation: forcing tumour progression. Nature reviews. Cancer. 2009; 9:108.
49. Xu R, Boudreau A, Bissell MJ. Tissue architecture and function: dynamic reciprocity via extraand intra-cellular matrices. Cancer metastasis reviews. 2009; 28:167. [PubMed: 19160017]

50. Ausubel, FM.; Brent, R.; Kingston, RE.; Moore, DD.; Seidman, JG.; Smith, JA.; Struhl, K. Current protocols in molecular biology. Ausubel, FM.; Brent, R.; Kingston, RE.; Moore, DD.; Seidman, JG.; Smith, JA.; Struhl, K., editors. New York, N.Y: John Wiley & Sons, Inc; 1987–2006.
51. Guthrie, C.; Fink, GR. Methods in Enzymology, Guide to Yeast Genetics and Molecular Biology. Guthrie, C.; Fink, GR., editors. California: Academic Press, San Diego; 1991. p. 92101
52. Yu RC, Pesce CG, Colman-Lerner A, Lok L, Pincus D, Serra E, Holl M, Benjamin K, Gordon A, Brent R. Negative feedback that improves information transmission in yeast signalling. Nature. 2008; 456:755. [PubMed: 19079053]
53. Cleveland, EGaWMSWS. Statistical Models in S. Hastie, JMCaTJ., editor. Wadsworth & Brooks/Cole; 1992.
54. Tarocco F, Lecuona RE, Couto AS, Arcas JA. Optimization of erythritol and glycerol accumulation in conidia of Beauveria bassiana by solid-state fermentation, using response surface methodology. Applied microbiology and biotechnology. 2005; 68:481. [PubMed: 15731900]
55. Pinheiro JC, Bates DM. Mixed-effects models in S and S-PLUS. 2000 Springer Verlag.
56. Ma W, Trusina A, El-Samad H, Lim WA, Tang C. Defining network topologies that can achieve biochemical adaptation. Cell. 2009; 138:760. [PubMed: 19703401]
57. Chambers, JM. Statistical Models in S. Wadsworth & Brooks/Cole; 1992. chap. 4
58. Sikorski RS, Hieter P. A system of shuttle vectors and yeast host strains designed for efficient manipulation of DNA in Saccharomyces cerevisiae. Genetics. 1989; 122:19. [PubMed: 2659436]

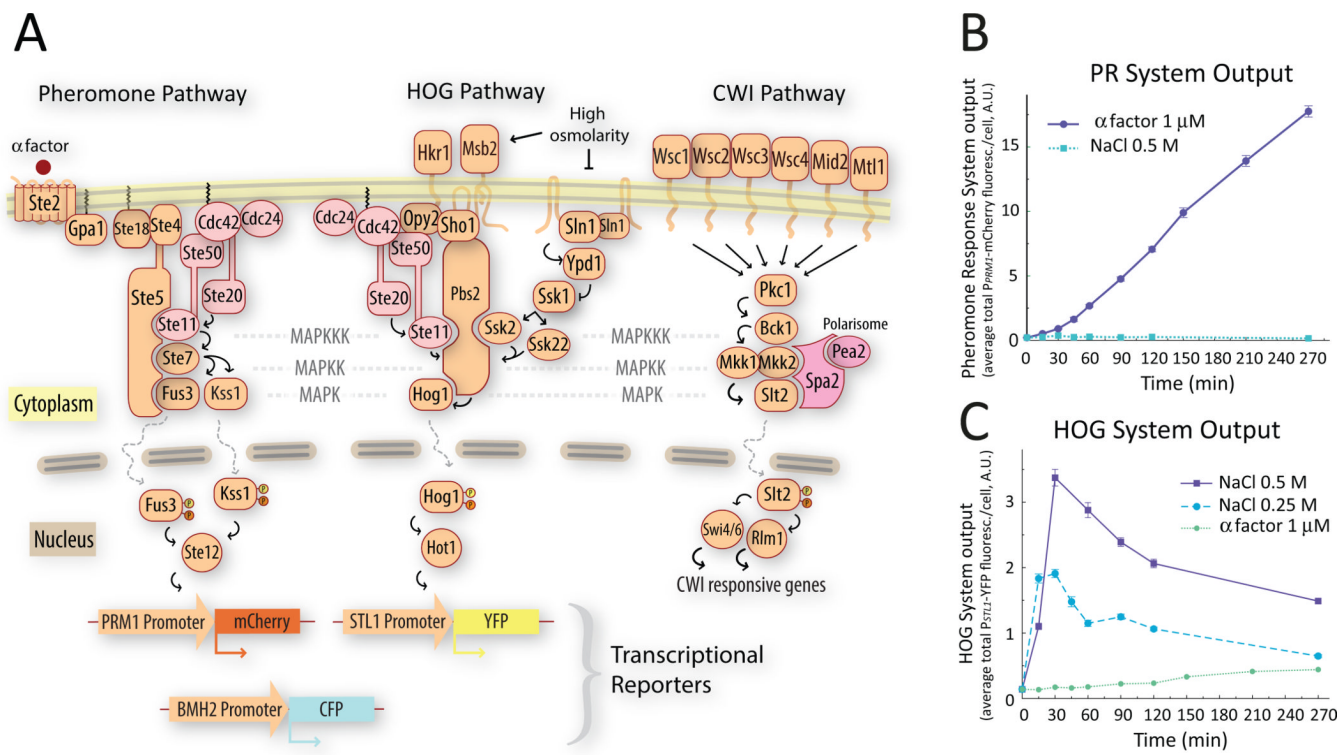

Figure 1. A. Schematic representation of the three MAPK pathways relevant for this study

Activation of the pheromone response pathway induces the P_{PRM1}-mCherry transcriptional reporter (left). When phosphorylated and activated Hog1 translocates to the nucleus, it associates with transcription factors like Hot1 to drive the expression of the P_{STL1}-YFP transcriptional reporter (middle). The CWI MAPK pathway (right). **B&C. Single stimulus behavior of the transcriptional reporters used in this study**. We stimulated exponentially growing wild-type (LD3342, Δ*bar1* P_{PRM1}-mCherry P_{STL1}-YFP P_{BMH2}-CFP) cells with α factor (**B**) or the indicated concentrations of NaCl (**C**), and collected samples into cycloheximide at the indicated times for imaging and fluorescent protein quantification. Each input activated only one reporter. Addition of NaCl caused an increase in YFP fluorescence followed by a decline to a lower steady state. Data corresponds to the average total mCherry (**B**) or YFP (**C**) fluorescence intensity per cell. Error bars represent the standard error of the mean. (n ~ 700 cells for each data point). Plots show one representative experiment out of three biological replicates.

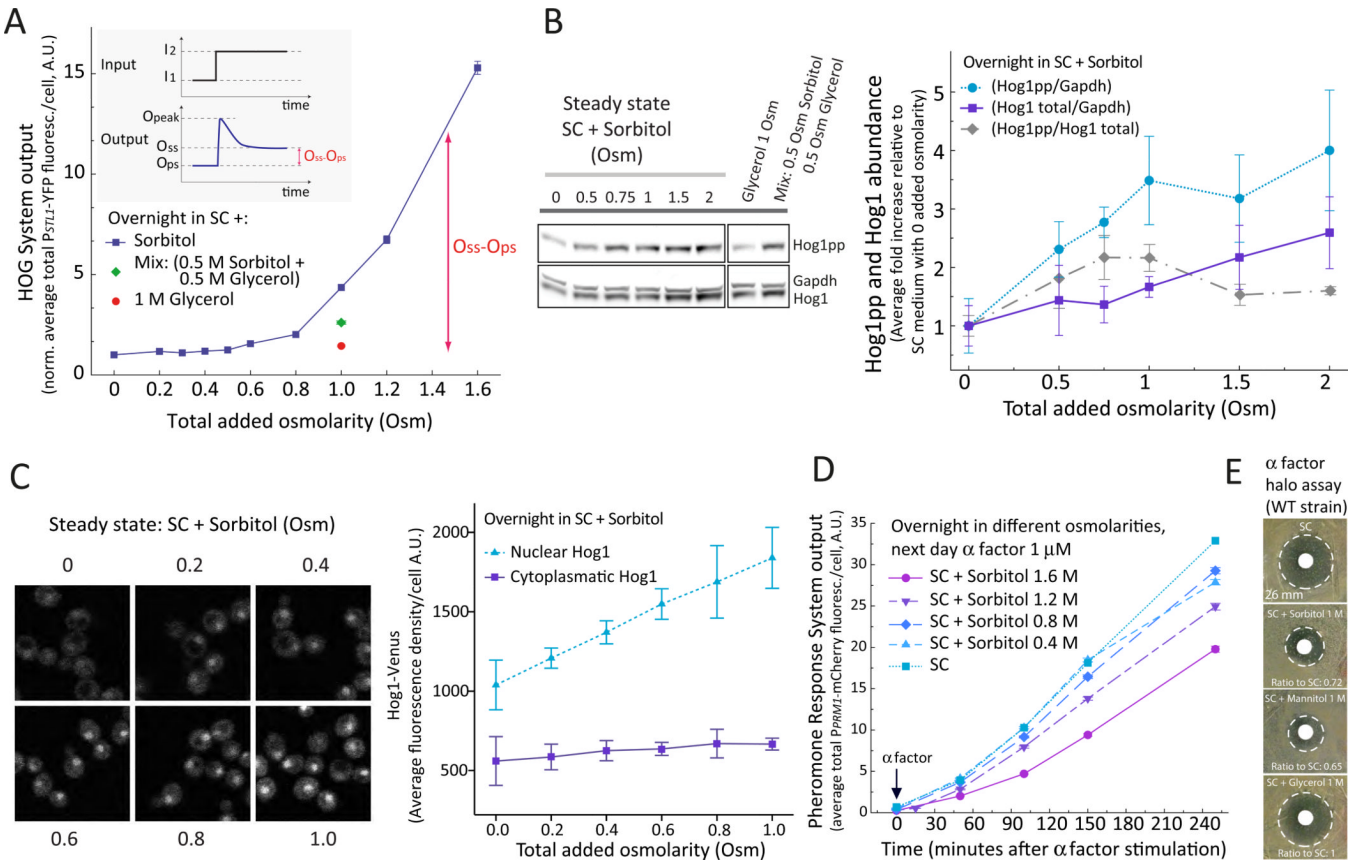

Figure 2. Steady state activity of HOG after adaptation is osmolarity dependent

A. HOG transcriptional output. Wild-type (LD3342) cells were adapted over-night to SC (synthetic complete) medium supplemented with sorbitol, glycerol or both osmotica as indicated. Data corresponds to the average total YFP fluorescence intensity per cell normalized to that in SC medium. The HOG adaptive response (inset). **I1**: Initial external osmolarity, **I2**: Final external osmolarity. **Ops**: HOG output pre-shock, **Opeak**: HOG output at maximum response, **Oss**: HOG output at steady state post shock. Nomenclature based on Ma *et al.* (56). Oss – Ops increases with the external osmolarity ($p < 1e-4$). Error bars represent SEM. n ~ 700 cells for each data point. **B. HOG phosphorylation**. LD3342 cells were cultured as in **A** and protein extracts were analyzed by WB. Representative WB using antibodies against the indicated proteins (left). Quantification of Hog1 phosphorylation in the indicated conditions (right). Data corresponds to the indicated ratios, normalized to values at 0 added Osm (N= 3 experiments). Hog1pp/Gadph and Hog1 total/Gadph increases with external osmolarity ($p = 0.016$ and 0.03, respectively). Hog1pp/Hog1 total between 0.5 and 1 Osm increases significantly with respect to 0 Osm ($\alpha = 0.05$, Tukey´s multiple contrasts) **C. HOG localization**. Wild type yeast (ySP69) expressing Hog1-Venus and Hta2-CFP were cultured as in A and Z-stacks were acquired in a confocal microscope. Montage of cells with in-focus nucleus (left). Quantitification of nuclear and cytoplasmic Hog1-Venus fluorescence intensity at the indicated osmolarity (right). Nuclear Hog1 increases with external osmolarity (76 +/− 4 %/Osm, $p < e-4$). Cytoplasmic Hog1 slightly increases with osmolarity (20 +/− 6 %/Osm $p=0.014$). See also Figure S2 and S3. Data corresponds to the mean +/− SEM (N = 3 experiments). **D. PR transcriptional output**. LD3342 cells were cultured as in **A** and treated with 1 μM α factor. At the indicated times samples were collected into cycloheximide for imaging and fluorescent protein quantification. Data corresponds to the mean total mCherry fluorescence intensity per cell +/

− SEM of one representative experiment (N = 3). n ~ 700 cells for each data point. The transcription rate of mCherry decreased with external osmolarity ($p < 1e-4$ for this experiment). **E. PR induced cell cycle arrest**. Images correspond to halo assays performed with LD3342 yeast on SC plates with the indicated added osmoticum. The doubling time of yeast in these different media was similar: 85.97 +/− 0.74 min (SC with no additions), 93.11 +/− 1.03 min (SC + 1 M sorbitol), 93.37 +/− 3.41 (SC + 1 M glycerol) and 91.00 +/− 3.84 min (SC + 1 M mannitol). See also Fig. S1 to S3.

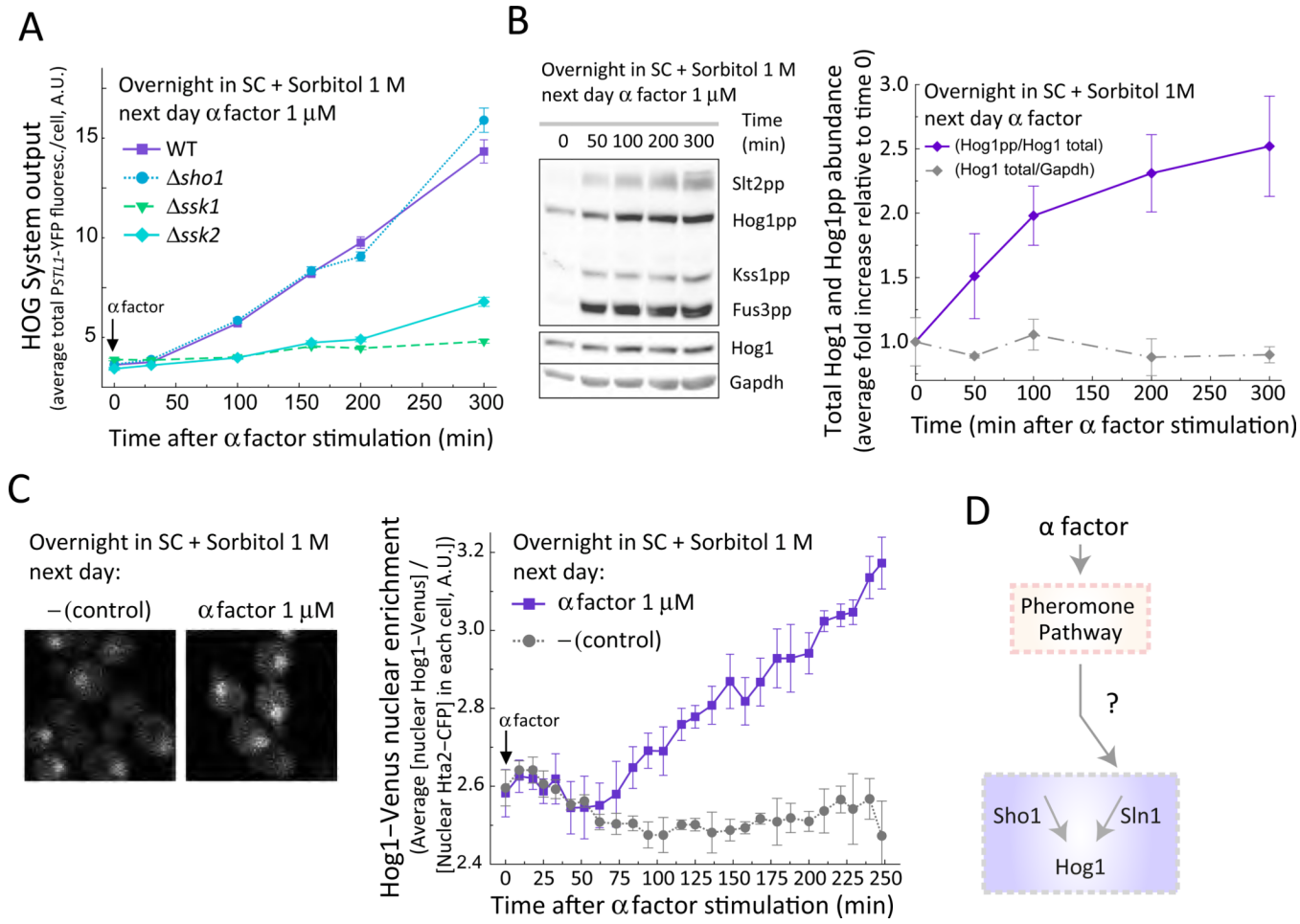

Figure 3. Mating pheromone activates HOG

A. HOG transcriptional output. Wild-type (LD3342), Δ*sho1* (RB3704), Δ*ssk1* (RB3382a) and Δ*ssk2* (RB3642) cells adapted to sorbitol were stimulated with α factor and collected into cycloheximide at the indicated time points for imaging. Data corresponds to the mean +/− SEM of the total YFP fluorescence intensity per cell normalized to time zero of one experiment (N = 3 experiments). (n ~ 700 cells for each data point). YFP fluorescence significantly increased 50 min after pheromone treatment for WT ($p < e\text{-}4$) and Δ*sho1* ($p < e\text{-}4$), but not for Δ*ssk1* ($p = 0.31$) or Δ*ssk2* ($p = 0.07$). **B. HOG phosphorylation**. Representative WB with protein extracts from LD3342 cells cultured as in **A** using antibodies against the indicated proteins (left). Quantification of Hog1 phosphorylation in the indicated conditions (right). Data corresponds to the mean +/− SEM of the indicated ratios, normalized to values at time zero (N = 3). Hog1-pp to total Hog1 increases after pheromone treatment ($p < e\text{-}4$). **C. HOG localization**. Wild-type yeast(ySP69) expressing Hog1-Venus and Hta2-CFP were cultured as in **A** and imaged in a confocal microscope. Montage showing cells with in-focus nucleus (left). Quantitification of nuclear Hog1-Venus fluorescence localization at the indicated osmolarity (right). Data corresponds to the mean +/− SEM ratio of the ratio of nuclear YFP to CFP signal (N = 3 experiments). Nuclear YFP to CFP ratio increases 50 min after pheromone treatment ($p < e\text{-}4$). **D**. Model of pheromone-dependent activation of HOG through stimulation of the Sln1 branch. See also Fig. S4 to S7.

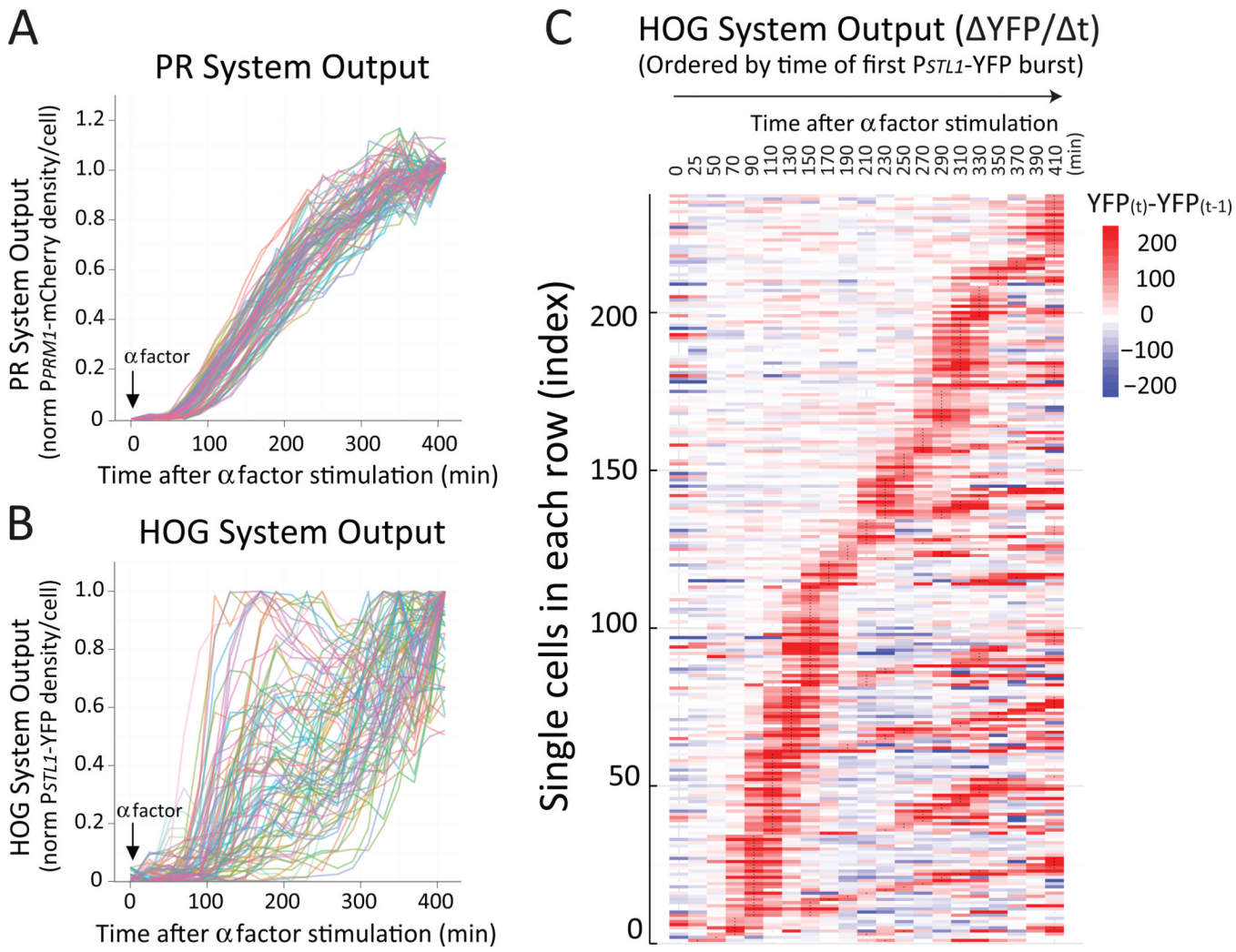

Figure 4. Pheromone-dependent activation of HOG occurs in unsynchronized bursts

Wild-type (LD3342) cells were adapted to sorbitol, attached to a glass-bottom 96-well plate and followed under the microscope after pheromone stimulation. PR (**A**) or HOG (**B**) transcriptional output in single cells. Each trace corresponds to mCherry (P_{PRM1}-mCherry, **A**) or YFP (P_{STL1}-YFP, **B**) fluorescence intensity over time, normalized to the maximum and minimum values for each cell. **C**. Heat-map representation of single cell HOG transcriptional output time-course profiles. Cells were ordered (bottom up) based on the time at which they showed their first burst of HOG activity and for those cells with equal burst time of first burst, sorted based on their second burst. ΔYFP/Δt, the time derivative of the YFP fluorescence density. See also Fig. S9 to S11.

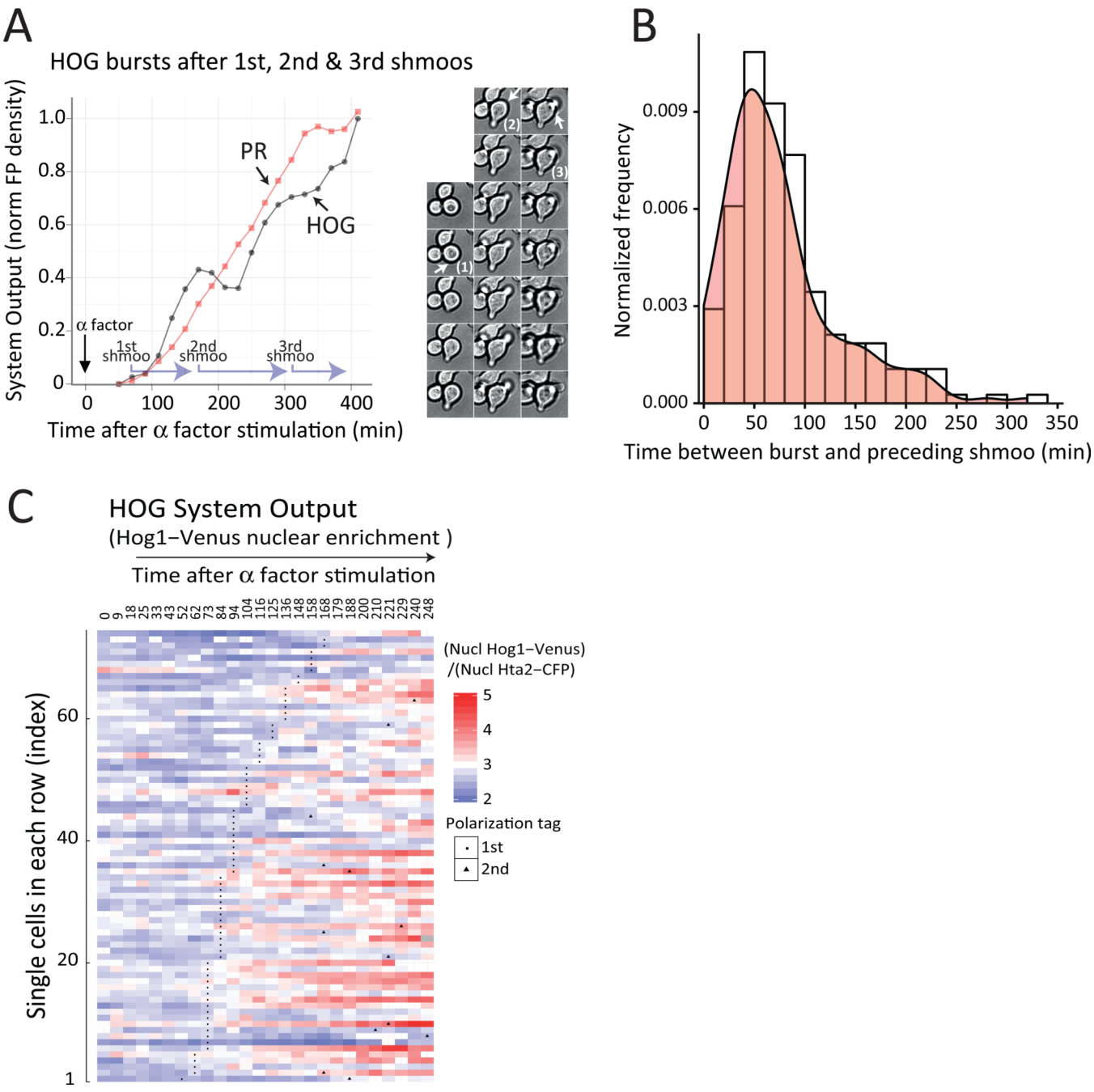

Figure 5. Pheromone-dependent activation of HOG correlates with shmooing

A. Time-course (left) of a cell with three bursts of HOG activity, selected from the time courses in Fig. 4 (see also Fig. S10 and S11). Plots show HOG and PR transcriptional output, overlaid with shmooing times (light purple L shaped arrows mark shmooing periods, starting at the time each mating projection is first apparent). Photomontage (right) shows the bright field time-lapse images used to determine the timing of shmooing. Numbers mark shmoos and arrows highlight the position of the nascent mating projection in each cell. Accumulation of the HOG reporter is slightly delayed (about 30 to 40 minutes) from the time of shmooing due to the slow (40 min) maturation of YFP (28). Data corresponds to the fluorescence intensity normalized to the maximum and minimum values. **B**. Distribution of

times between the first frame at which a shmoo was detectable and the time of the peak expression (highest ΔYFP/At) of the subsequent HOG burst. **C**. Heat-map representation of single cell Hog1-venus nuclear localization time-course profiles from Fig. 3C. Cells were ordered (bottom up) based on the time they show their first shmoo (black dots). Data corresponds to nuclear YFP over CFP signal at each time point, which is significantly higher after shmoo formation than before ($p < e\text{-}4$)

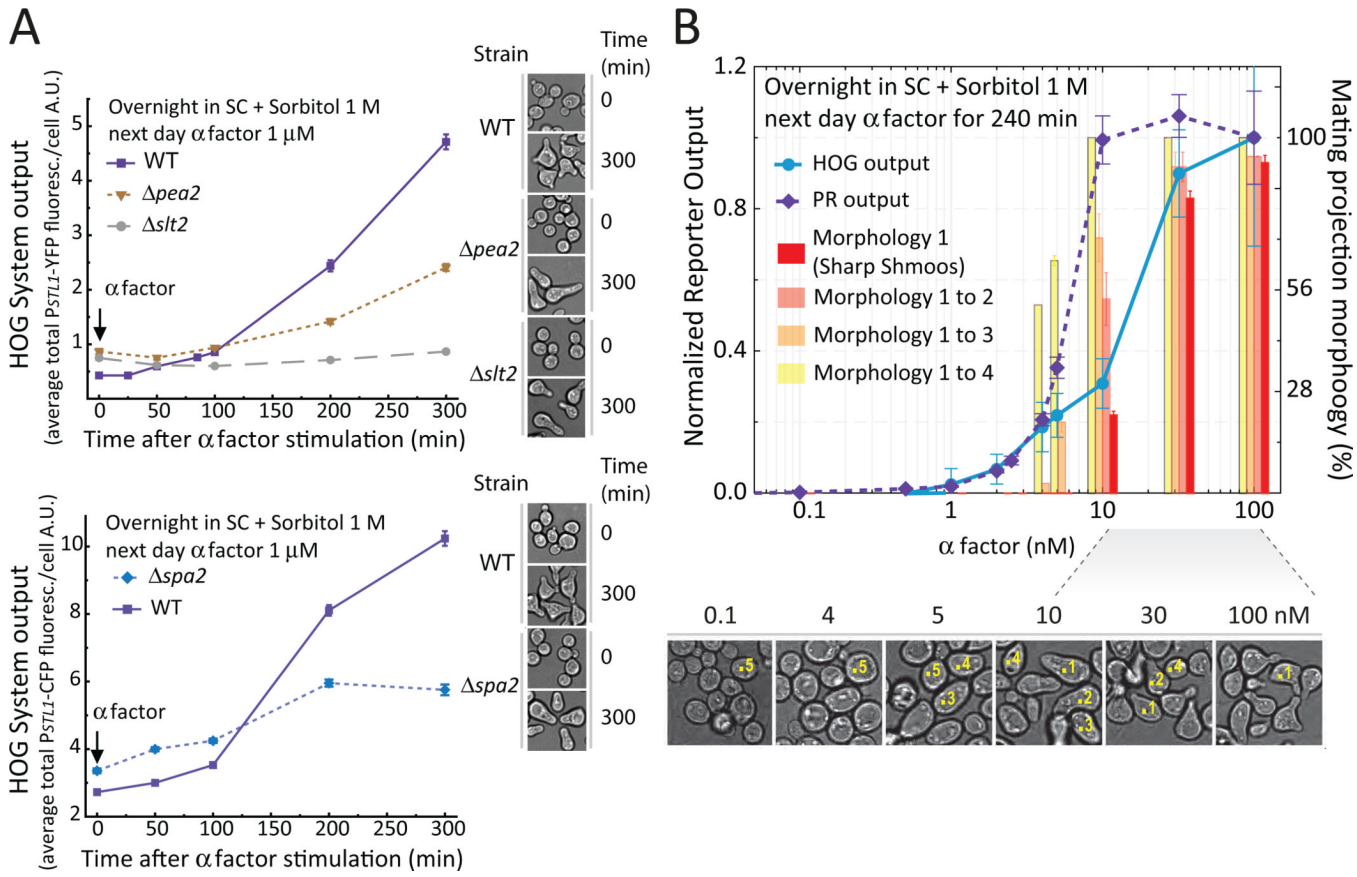

Figure 6. Pheromone-dependent HOG activation requires an intact polarisome and the CWI MAPK Slt2

A. Wild-type (LD3342 or RB3406), *Δpea2* (RB3862), *Δspa2* (RB3865) and *Δslt2* (RB3376a) cells were cultured as in Fig. 3, stimulated with pheromone and collected for imaging in cycloheximide. Data corresponds to the HOG reporter expression average +/− SEM YFP (top) or CFP (bottom) fluorescence intensity per cell over time. HOG reporter expression is reduced in *Δpea2* ($p < e\text{-}4$), *Δspa2* ($p = 0.0097$) and *Δslt2* ($p < e\text{-}4$) as compared to the correspondent WT strains.Images of each strain at time 0 and 300 min after pheromone stimulation are also shown. Note the typical "peanut" morphology of the polarisome mutants. **B**. Wild-type (LD3342) cells were cultured as in Fig. 3, stimulated with the indicated pheromone concentrations, and collected for imaging in cycloheximide. Data corresponds to the average +/− SEM YFP (circles) or mCherry (diamonds) normalized to maximum value (left Y axis); or the percentage +/− SD of cells with the different mating projection morphology categories (from 1 to 4), aggregated as indicated (right Y axis). The effective concentration of half maximal response (EC_{50}) for the HOG output differs significantly from the PR output ($p < e\text{-}4$), but not from the fraction of “sharp shmoos” ($p = 0.64$). Sample bright field images are shown below the plot. Numbers on top of selected cells illustrate the morphology classification used (category 5 corresponds to dividing cells). Note that sharp shmoos (category 1) form only above 10 nM. One representative experiment ($N > 3$). $n \sim 700$ cells for each data point. See also Fig. S12 and S13.

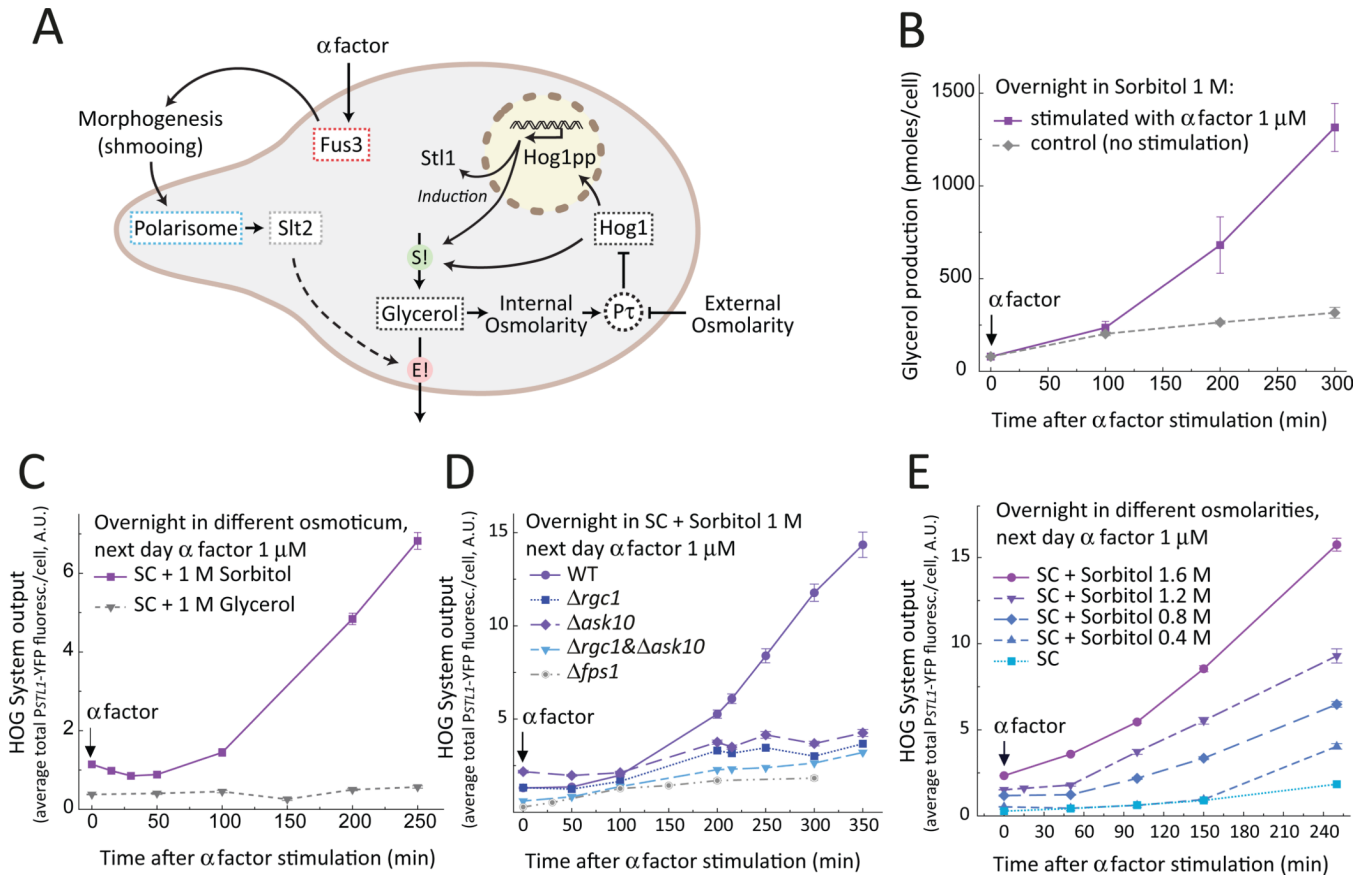

Figure 7. Pheromone activates HOG by stimulating glycerol loss

A. Schematic model of HOG activation by pheromone in cells growing in a high osmolarity environment. Addition of pheromone (or the presence of a mating partner) activates the MAPK Fus3, leading to the mating projection formation (“shmooing”). The machinery involved in shmooing (the polarisome) and cell wall stress activate the CWI pathway and its MAPK Slt2. Activated Fus3 together with Slt2 increase glycerol loss. Intracellular glycerol is required to maintain normal turgor pressure (**Pτ**). The pheromone-induced loss of glycerol (**E!**) results in low turgor pressure and in activation of HOG, leading to a compensatory increase in the glycerol synthesis rate (**S!**) accomplished by HOG activity. **B–E**. Testing four predictions of the model in **A. B. Extracellular accumulation of glycerol**. Wild-type (LD3342) cells were cultured overnight in sorbitol and collected at the indicated times from cultures stimulated (squares) or not (diamonds) with pheromone to measure the amount of glycerol in the supernatant. Data corresponds to the average concentration of glycerol in the supernatant divided by the number of cells at each time point (see Figure S15). Bars represent standard deviation (N = 3 independent experiments). Glycerol production is significantly increased in pheromone treated cells ($p = 0.0028$). **C. Replacement of sorbitol by glycerol as extracellular osmoticum**. Wild type (LD3342) cells was cultured overnight in sorbitol (squares) or glycerol (triangles), stimulated with pheromone, and samples were collected into cycloheximide at the indicated times to measure reporter expression by microscopy. The HOG reporter was induced in the sorbitol adapted cells ($p < e\text{-}4$), but not in the glycerol adapted ones ($p = 0.39$). **D. Pheromone-mediated HOG activation requires the aquaglyceroporin Fps1**. Wild-type (LD3342), Δ*fps1* (RB3396a), Δ*rgc1* (RB3710), Δ*ask10* (RB3717) and Δ*rgc1* Δ*ask10* (RB3722) cells were cultured overnight with 1M sorbitol, stimulated with pheromone and collected into cycloheximide to measure reporter

gene expression by microscopy. All mutants had significantly lower HOG reporter transcription than WT cells ($p < 1e-4$). **E. Pheromone-mediated HOG activation increases with increased external osmolarity**. Wild-type (LD3342) cells were cultured overnight in the indicated concentrations of sorbitol, stimulated with pheromone and collected into cycloheximide to measure reporter gene expression by microscopy. YFP transcription rate increased with external osmolarity ($p < e-4$). **C–E**. Data corresponds to the average YFP fluorescence intensity per cell +/− SEM of one representative experiment. N = 3 experiments in all panels. n ~ 700 cells for each data point. P-values calculated for the shown data.

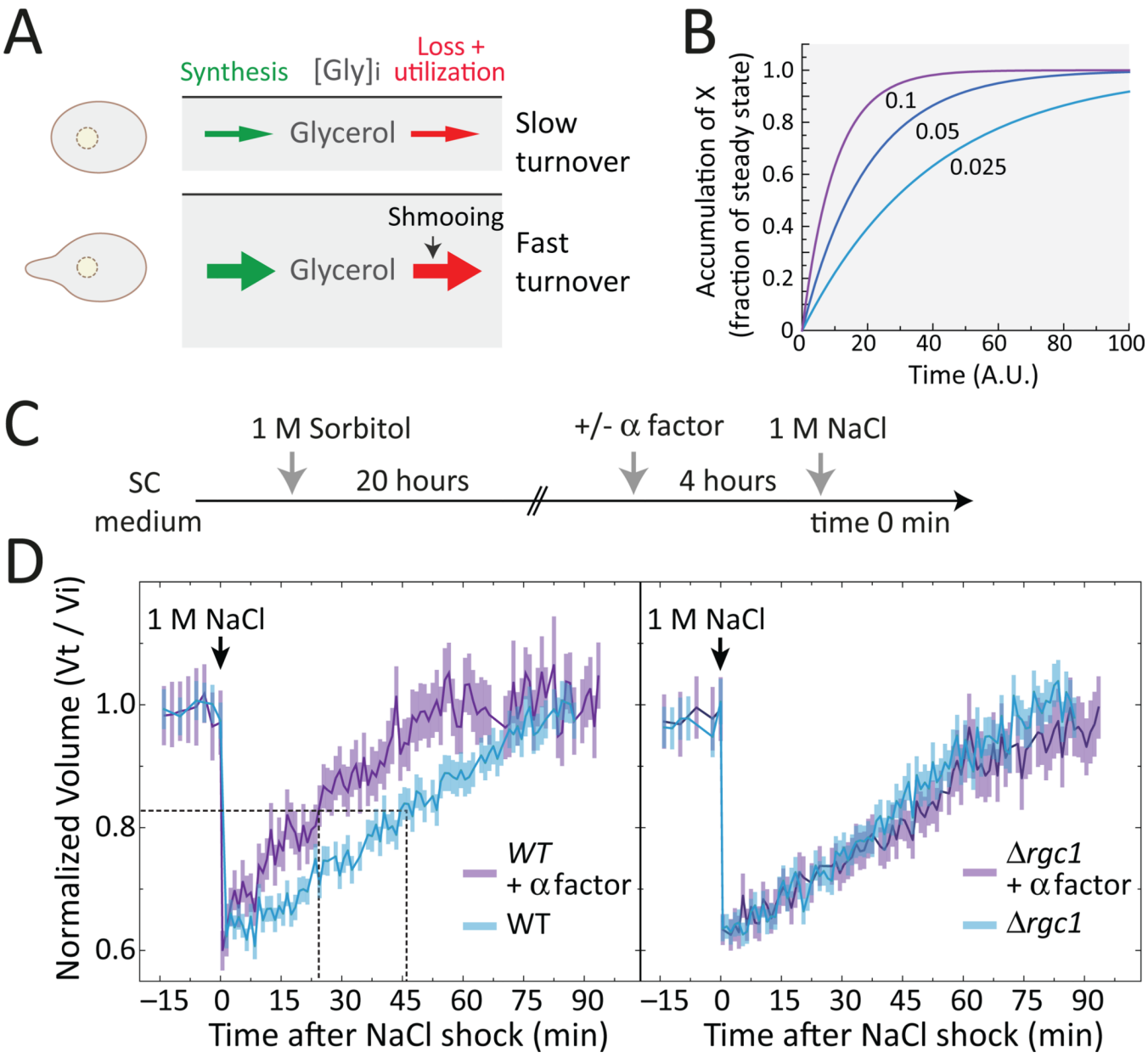

Figure 8. Pheromone stimulated cells display improved osmoadaptation

A. Cells maintain an internal glycerol concentration depending on the external osmolarity. In the absence of pheromone, glycerol concentration has a given turnover rate. Pheromone increases the rate of glycerol loss, accelerating its turnover rate. **B**. The effect of the turnover rate on the dynamics of a putative system in which molecule X is synthesized at a rate β and lost/degraded at a rate **a**, following the equation dX/dt = β -aX. The plot shows ts the dynamics of this system starting at X = 0, for three different values of β and **a** (0.1, 0.05 and 0.025 in units of 1/time). The faster the turnover rate, the faster the system reaches steady-state. **C**. Cells cultured overnight in sorbitol were stimulated with pheromone, then NaCl was added and cell volume was monitored by microscopy. **D**. Wild-type (LD3342) (left) or *Δrgc1* (RB3710) (right) cells. Data corresponds to the average +/− SEM volume normalized to time zero. The horizontal dotted line marks 50% volume recovery. The vertical dotted line marks the time at which this recovery was achieved. Wild-type cells treated with

pheromone recover faster than untreated cells (p = 0.0083), but *Δrgc1* do not (p = 0.88). See also Fig. S16. N = 3 experiments.